

Electrochemical Reduction of Carbon Dioxide to Formate on Bi and BiSn Electrodes  
Prepared by Electrodeposition on Copper Foil



A Thesis Submitted in Partial Fulfillment of the Requirements  
for the Degree of Master of Engineering in Chemical Engineering

Department of Chemical Engineering

FACULTY OF ENGINEERING

Chulalongkorn University

Academic Year 2020

Copyright of Chulalongkorn University

การรีดักชันทางเคมีไฟฟ้าของแก๊สคาร์บอนไดออกไซด์ไปสู่ฟอร์มเมตบนตัวเร่งปฏิกิริยาบิสมัทและบิสมัท  
ผสมดีบุกเตรียมโดยการพอกพูนทางไฟฟ้าบนแผ่นทองแดง



วิทยานิพนธ์นี้เป็นส่วนหนึ่งของการศึกษาตามหลักสูตรปริญญาวิทยาศาสตรมหาบัณฑิต  
สาขาวิชาวิศวกรรมเคมี ภาควิชาวิศวกรรมเคมี  
คณะวิศวกรรมศาสตร์ จุฬาลงกรณ์มหาวิทยาลัย  
ปีการศึกษา 2563  
ลิขสิทธิ์ของจุฬาลงกรณ์มหาวิทยาลัย

Thesis Title                      Electrochemical Reduction of Carbon Dioxide to  
Formate on Bi and BiSn Electrodes Prepared by  
Electrodeposition on Copper Foil  
By                                      Miss Jutamas Wasombut  
Field of Study                      Chemical Engineering  
Thesis Advisor                      Professor JOONGJAI PANPRANOT, Ph.D.

---

Accepted by the FACULTY OF ENGINEERING, Chulalongkorn University in  
Partial Fulfillment of the Requirement for the Master of Engineering

..... Dean of the FACULTY OF  
ENGINEERING  
(Professor SUPOT TEACHAVORASINSKUN, D.Eng.)

THESIS COMMITTEE

..... Chairman  
(Assistant Professor AMORNCHAI ARPORNWICHANOP,  
D.Eng.)

..... Thesis Advisor  
(Professor JOONGJAI PANPRANOT, Ph.D.)

..... Examiner  
(Chutimon Satirapipathkul, Ph.D.)

..... External Examiner  
(Patcharaporn Weerachawanasak, Ph.D.)

จุฬามาศ วะสมบัติ : การรีดักชันทางเคมีไฟฟ้าของแก๊สคาร์บอนไดออกไซด์ไปสู่ออร์เมตบนตัวเร่งปฏิกิริยาบิสมัทและบิสมัทผสมดีบุกเตรียมโดยการพอกพูนทางไฟฟ้าบนแผ่นทองแดง. ( Electrochemical Reduction of Carbon Dioxide to Formate on Bi and BiSn Electrodes Prepared by Electrodeposition on Copper Foil) อ.ที่ปรึกษาหลัก : ศ. ดร.จุงใจ ปั้นประณต

ในงานวิจัยนี้ศึกษาตัวเร่งปฏิกิริยาทางไฟฟ้าโลหะบิสมัท/ทองแดงที่เตรียมโดยการพอกพูนทางไฟฟ้าของบิสมัทบนแผ่นทองแดงและตัวเร่งปฏิกิริยาทางไฟฟ้าโลหะผสมบิสมัทดีบุก/ทองแดงที่เตรียมโดยการพอกพูนทางไฟฟ้าของบิสมัทและดีบุกบนแผ่นทองแดงในอ่างพอกพูนทางไฟฟ้าที่ความเข้มข้นของบิสมัทไอออนแตกต่างกันได้แก่ 0.05, 0.1 และ 0.2 โมลาร์ ในขณะที่ความเข้มข้นของดีบุกไอออนคงที่ที่ 0.025 โมลาร์ เพื่อใช้ในปฏิกิริยารีดักชันทางไฟฟ้าของแก๊สคาร์บอนไดออกไซด์ วิเคราะห์ตัวเร่งปฏิกิริยาทางกายภาพและองค์ประกอบทางเคมีด้วยเทคนิคกล้องจุลทรรศน์อิเล็กตรอนแบบส่องกราดร่วมกับเอ็กซ์เรย์สเปกโตรสโกปีแบบกระจายพลังงาน เทคนิคเอ็กซ์เรย์โฟโตอิเล็กตรอนสเปกโตรสโกปีและเทคนิคการเลี้ยวเบนของรังสีเอ็กซ์ ผลการทดสอบพบว่าความเข้มข้นของบิสมัทและดีบุกส่งผลต่อโครงสร้างของตัวเร่งปฏิกิริยาบิสมัทที่แตกต่างกันในรูปแบบบัลคก็และแบบพื้นผิวขรุขระ สำหรับการทดสอบปฏิกิริยารีดักชันทางไฟฟ้าของแก๊สคาร์บอนไดออกไซด์ แก๊สไฮโดรเจนและคาร์บอนมอนอกไซด์ถูกตรวจพบในผลิตภัณฑ์แก๊สในขณะที่ผลิตภัณฑ์ของเหลวหลักคือฟอร์มेटดังแสดงจากการวิเคราะห์ด้วยเทคนิคนิวเคลียร์แมกเนติกเรโซแนนซ์ ตัวเร่งปฏิกิริยาบิสมัท<sub>0.1</sub>/ทองแดงเป็นตัวเร่งปฏิกิริยาทางไฟฟ้าที่ผลิตฟอร์มेटได้ดีที่สุดที่ความต่างศักย์ -1.8 โวลต์เทียบกับซิลเวอร์/ซิลเวอร์คลอไรด์ โดยมีอัตราการผลิตฟอร์มेटสูงสุด 5.41 ไมโครโมลต่อนาที่ต่อตารางเซนติเมตร นอกจากนี้ตัวเร่งปฏิกิริยาบิสมัท<sub>0.1</sub>/ทองแดง มีเสถียรภาพที่ดีในการทดสอบเป็นเวลา 10 ชั่วโมง โดยพบประสิทธิภาพการผลิตฟอร์มेटที่สูงกว่าร้อยละ 80 ตลอดการทดลอง แม้ภายหลังการทดลองอนุภาคของบิสมัทบัลคก็มีรูปร่างที่เปลี่ยนไปเล็กน้อยจากการเกิดสารประกอบบิสมัทซึบคาร์บอนเนต

สาขาวิชา วิศวกรรมเคมี

ลายมือชื่อนิสิต .....

ปีการศึกษา 2563

ลายมือชื่อ อ.ที่ปรึกษาหลัก .....

# # 6270041621 : MAJOR CHEMICAL ENGINEERING

KEYWORD: Electrochemical carbon dioxide reduction, Bismuth catalyst,  
Electrodeposition, Formate production

Jutamas Wasombut : Electrochemical Reduction of Carbon Dioxide to Formate on Bi and BiSn Electrodes Prepared by Electrodeposition on Copper Foil. Advisor: Prof. JOONGJAI PANPRANOT, Ph.D.

In this study, The  $\text{Bi}_x/\text{Cu}$  electrocatalysts were prepared by electrodeposition of Bi on Cu foil, and the  $\text{Bi}_x\text{Sn}_y/\text{Cu}$  electrocatalysts were prepared by electrodeposition of Bi and Sn on Cu foil in deposition solution bath with different  $\text{Bi}^{3+}$  ion concentrations of 0.05, 0.1, and 0.2 M ( $\text{Bi}_{0.05}/\text{Cu}$ ,  $\text{Bi}_{0.1}/\text{Cu}$ ,  $\text{Bi}_{0.2}/\text{Cu}$ ), while the  $\text{Sn}^{2+}$  ion concentration was constant at 0.025 M ( $\text{Bi}_{0.05}\text{Sn}_{0.025}/\text{Cu}$ ,  $\text{Bi}_{0.1}\text{Sn}_{0.025}/\text{Cu}$ ,  $\text{Bi}_{0.2}\text{Sn}_{0.025}/\text{Cu}$ ). The electrocatalysts were characterized by SEM-EDX, XRD, and XPS and tested in the electrochemical  $\text{CO}_2$  reduction reaction. The results demonstrate that the Bi concentrations in the deposition bath affect the structure of Bi into different forms, including bulky structure and rough surface. Under the electrochemical  $\text{CO}_2$  reduction reaction experiments,  $\text{H}_2$  and CO were detected in the gas products, while formate was a major liquid product as confirmed by NMR analysis. The  $\text{Bi}_{0.1}/\text{Cu}$  electrocatalyst gives the best catalytic performance for formate formation at a potential of -1.8 V vs. Ag/AgCl with a high formate production rate of  $5.41 \mu\text{mol}/\text{min}\cdot\text{cm}^2$ . In addition, the  $\text{Bi}_{0.1}/\text{Cu}$  electrocatalyst was highly stable with FE<sub>formate</sub> above 80% for 10 hours, although the Bi bulky particles had slightly changed after reaction due to the formation of  $\text{Bi}_2\text{O}_2\text{CO}_3$  species.

Field of Study: Chemical Engineering

Student's Signature .....

Academic Year: 2020

Advisor's Signature .....

## ACKNOWLEDGEMENTS

This thesis would not be completed without the encouragement and support from these people, whom I wish to acknowledge here.

I appreciate my advisor, Professor Joongjai Panpranot for giving me support, suggestion, assistance, and encouragement to complete my thesis. In addition, I would be grateful to Assistant Professor Amornchai Arpornwichanop, as the chairman, Dr. Chutimon Satirapipathkul, and Dr. Patcharaporn Weerachawanasak as a member of the thesis committee for their valuable recommendations on this thesis.

I would like to acknowledge my colleagues for their excellent collaboration. Moreover, I could have never done this thesis without the support and encouragement from my lovely family.

Finally, The financial support from The Malaysia-Thailand Joint Authority (MTJA) is gratefully acknowledged.

Jutamas Wasombut



จุฬาลงกรณ์มหาวิทยาลัย  
CHULALONGKORN UNIVERSITY

## TABLE OF CONTENTS

	Page
ABSTRACT (THAI).....	iii
ABSTRACT (ENGLISH).....	iv
ACKNOWLEDGEMENTS .....	v
TABLE OF CONTENTS .....	vi
LIST OF TABLES .....	viii
LIST OF FIGURES .....	x
CHAPTER 1.....	1
INTRODUCTION.....	1
1.1. Introduction.....	1
1.2. Objectives of The Research .....	2
1.3. Scopes of the Research .....	2
CHAPTER 2.....	4
BACKGROUND AND LITERATUR REVIEWS.....	4
2.1. Fundamental of Electrochemical CO <sub>2</sub> Reduction .....	4
2.2. Study on Formate Formation on Electrodes.....	5
2.3. Study on Electrodeposition of Bi and BiSn Electrocatalysts.....	15
CHAPTER 3.....	23
MATERIALS AND METHODS .....	23
3.1. Materials.....	23
3.2. Catalysts Preparation.....	24
3.2.1. Preparation of copper foil.....	24

3.2.2. Preparation of $\text{Bi}_x/\text{Cu}$ electrocatalysts.....	24
3.2.3. Preparation of $\text{Bi}_x\text{Sn}_y/\text{Cu}$ electrocatalysts.....	25
3.3. Catalysts Characterization .....	26
3.3.1. Scanning electron microscope combined with energy dispersive X-ray spectroscopy (SEM/EDX) .....	26
3.3.2. X-ray photoelectron spectroscopy (XPS).....	26
3.3.3 X-ray diffraction (XRD).....	26
3.4. Electrochemical Reduction of $\text{CO}_2$ .....	27
3.5. Research methodology .....	29
CHAPTER 4.....	31
RESULTS AND DISCUSSION.....	31
4.1. Characterization of $\text{Bi}_x/\text{Cu}$ and $\text{Bi}_x\text{Sn}_y/\text{Cu}$ electrocatalyst with various concentrations.....	31
4.2 Electrochemical studies.....	40
CHAPTER 5.....	56
CONCLUSIONS .....	56
5.1 Conclusions .....	56
5.2 Recommendation.....	56
REFERENCES .....	57
VITA.....	69



## LIST OF TABLES

	Page
Table 1 Pd-based electrode in electrochemical reduction of CO <sub>2</sub> .....	7
Table 2 Pb-based electrode in electrochemical reduction of CO <sub>2</sub> .....	8
Table 3 In-based electrode in electrochemical reduction of CO <sub>2</sub> .....	9
Table 4 Sn-based electrode in electrochemical reduction of CO <sub>2</sub> .....	10
Table 5 Bi-based electrode in electrochemical reduction of CO <sub>2</sub> .....	12
Table 6 Bi electrodes prepared by electrodeposition.....	17
Table 7 BiSn electrodes prepared by electrodeposition .....	21
Chemicals used as precursors and electrolyte are listed in Table 8. ....	23
Table 9 Metals used as electrodes in electrodeposition method and electrochemical reduction of CO <sub>2</sub> .....	24
Table 10 Compositions of electrodeposition solutions for Bi <sub>x</sub> /Cu and Bi <sub>x</sub> Sn <sub>y</sub> /Cu Electrodes. ....	25
Table 11 The operating conditions of gas chromatograph with a thermal conductivity detector .....	28
Table 12 Weight percent and atomic percent of Bi <sub>x</sub> /Cu and Bi <sub>x</sub> Sn <sub>y</sub> /Cu electrocatalysts .....	31
Table 13 EMF <sup>0</sup> <sub>cell</sub> of electrodes.....	34
Table 14 the onset potential of each electrocatalyst .....	40
Table 15 The catalytic performances of Cu foil, Sn foil and Bi foil .....	44
Table 16 The catalytic performances of Bi <sub>x</sub> /Cu electrocatalysts with different Bi concentration .....	45
Table 17 The catalytic performances of Bi <sub>x</sub> Sn <sub>y</sub> /Cu electrocatalysts with different Bi concentration .....	46

Table 18 The stability performances of $\text{Bi}_{0.1}/\text{Cu}$ .....	52
--	----



## LIST OF FIGURES

	Page
Figure 1 Schematic of the electrochemical CO <sub>2</sub> reduction process and possible products.....	4
Figure 2 Mechanism for the electrochemical reduction of CO <sub>2</sub> to formate/ formic acid on metal surface. (A) mono- or bi-dentate intermediate route. (B) CO <sub>2</sub> <sup>-</sup> radical route.	6
Figure 3 Schematic representation of steps in the cathodic deposition of metals.....	16
Figure 4 Schematic of preparation of Bi <sub>x</sub> /Cu and Bi <sub>x</sub> Sn <sub>y</sub> /Cu electrocatalysts.....	26
Figure 5 Schematic of electrochemical reduction of CO <sub>2</sub> system.....	28
Figure 6 SEM images of (a) Cu foil, (b) Bi <sub>0.05</sub> /Cu, (c) Bi <sub>0.1</sub> /Cu, (d) Bi <sub>0.2</sub> /Cu, (e) Bi <sub>0.05</sub> Sn <sub>0.025</sub> /Cu, (f) Bi <sub>0.1</sub> Sn <sub>0.025</sub> /Cu and (g) Bi <sub>0.2</sub> Sn <sub>0.025</sub> /Cu.....	33
Figure 7 Bi 4f XPS spectra of (a) Bi <sub>0.05</sub> /Cu, (b) Bi <sub>0.1</sub> /Cu, and (c) Bi <sub>0.2</sub> /Cu electrodes.....	36
Figure 8 Bi 4f XPS spectra of (a) Bi <sub>0.05</sub> Sn <sub>0.025</sub> /Cu, (b) Bi <sub>0.1</sub> Sn <sub>0.025</sub> /Cu, and (c) Bi <sub>0.2</sub> Sn <sub>0.025</sub> /Cu electrodes.....	37
Figure 9 XRD pattern of (a) Bi <sub>0.05</sub> /Cu, (b) Bi <sub>0.1</sub> /Cu, (c) Bi <sub>0.2</sub> /Cu, (d) Bi <sub>0.05</sub> Sn <sub>0.025</sub> /Cu, (e) Bi <sub>0.1</sub> Sn <sub>0.025</sub> /Cu and (f) Bi <sub>0.2</sub> Sn <sub>0.025</sub> /Cu.....	39
Figure 10 LSV curve of Bi <sub>0.05</sub> /Cu electrode.....	41
Figure 11 LSV curve of Bi <sub>0.1</sub> /Cu electrode.....	42
Figure 12 LSV curve of Bi <sub>0.2</sub> /Cu electrode.....	42
Figure 13 LSV curve of Bi <sub>0.05</sub> Sn <sub>0.025</sub> /Cu electrode.....	43
Figure 14 LSV curve of Bi <sub>0.1</sub> Sn <sub>0.025</sub> /Cu electrode.....	43
Figure 15 LSV curve of Bi <sub>0.2</sub> Sn <sub>0.025</sub> /Cu electrode.....	44
Figure 16 SEM images of (a) Bi <sub>0.05</sub> /Cu, (b) Bi <sub>0.1</sub> /Cu, (c) Bi <sub>0.2</sub> /Cu, (d) Bi <sub>0.05</sub> Sn <sub>0.025</sub> /Cu, (e) Bi <sub>0.1</sub> Sn <sub>0.025</sub> /Cu and (f) Bi <sub>0.2</sub> Sn <sub>0.025</sub> /Cu after reaction.....	50

Figure 17 XRD pattern of (a) $\text{Bi}_{0.05}/\text{Cu}$ , (b) $\text{Bi}_{0.1}/\text{Cu}$ , (c) $\text{Bi}_{0.2}/\text{Cu}$ , (d) $\text{Bi}_{0.05}\text{Sn}_{0.025}/\text{Cu}$ , (e) $\text{Bi}_{0.1}\text{Sn}_{0.025}/\text{Cu}$ and (f) $\text{Bi}_{0.2}\text{Sn}_{0.025}/\text{Cu}$ after reaction .....	51
Figure 18 Current density and $\text{FE}_{\text{formate}}$ during stability test .....	53
Figure 19 SEM images of $\text{Bi}_{0.1}/\text{Cu}$ (a) before and (b) after stability test .....	54
Figure 20 XRD patterns of $\text{Bi}_{0.1}/\text{Cu}$ (a) before and (b) after stability test .....	55



# CHAPTER 1

## INTRODUCTION

### 1.1. Introduction

Nowadays, the accelerated exhaustion of fossil fuels from the overgrowth of economics has increasingly released and accumulated greenhouse gas such as carbon dioxide ( $\text{CO}_2$ ) in the atmosphere that contributed to global warming. [1],[2],[3] This environmental problem has become a critical awareness issue in public society that is concerned by governments worldwide, therefore, carbon dioxide reduction for sustainable development has been studied. The conversion of  $\text{CO}_2$  to high value-added chemicals is an interesting way to mitigate these problems as carbon dioxide can be used as a major carbon resource. There are several methods for  $\text{CO}_2$  conversion, such as thermochemical reduction [4], photocatalytic reduction [5], photoelectrocatalysis reduction [6],[7], and electrochemical reduction of  $\text{CO}_2$  [8],[9], [10]. Among many methods, electrochemical  $\text{CO}_2$  reduction is expedient because this process is easy to control. Moreover, the process can be powered by clean and sustainable electricity sources.

However, the electrochemical reduction of carbon dioxide has some significant obstacles such as the stability of  $\text{CO}_2$  with low electron affinity (EA) and large energy gap between its molecular orbital leading to very slow reaction kinetics. Furthermore, hydrogen evolution reaction (HER) as a competitive reaction causes less  $\text{CO}_2$  reduction.[2],[11],[12] To achieve this challenge, studies on the high activity of electrocatalyst are important. Depending on the different catalyst materials and reaction conditions,  $\text{CO}_2$  can be reduced to a variety of useful products, such as carbon monoxide (CO), methane ( $\text{CH}_4$ ), methanol ( $\text{CH}_3\text{OH}$ ), ethylene ( $\text{C}_2\text{H}_4$ ), ethanol ( $\text{C}_2\text{H}_5\text{OH}$ ), and formate ( $\text{HCOO}^-$ ).[2],[13],[14] Among many products, formate is widely used in industry as feedstock, a hydrogen storage material, and a reactant in formic acid fuel cells.[15]

Electrocatalysts with high selectivity for formate production are mostly metal-based catalysts, including Pd, Pb, In, Sn, Bi. [3],[16],[17] Among them, Bismuth (Bi) is the most interesting because of its low toxicity, inexpensive, and high formate selectivity.

It was reported that Bi dendrite [15], [18],[19] , Bi nanoparticles [20],[21],[22] and Bi nanosheets [15],[23] could provide high formate selectivity. Meanwhile, the Sn-based catalyst is also interesting due to its very high stability, good formate selectivity, and low hydrogen production.[24],[25],[26] In previous studies, some researchers presented that Bi-Sn bimetallic forms exhibited a remarkable formate faradaic efficiency of over 90%.[11],[12],[27]

In this work, Bi-based electrocatalysts were prepared by electrodeposition method. Bi and bismuth-tin (Bi-Sn) were grown on copper (Cu) foil with various concentrations to fabricate  $\text{Bi}_x/\text{Cu}$  and  $\text{Bi}_x\text{Sn}_y/\text{Cu}$  for efficient formate production in the electrochemical reduction of  $\text{CO}_2$  reaction. The electrodeposition method is simple, harmless, easy, and suitable to prepare catalysts for the industry. The morphology, bulk composition, and crystalline structure of catalysts were characterized by X-ray diffraction analysis (XRD), X-ray photoelectron spectroscopy (XPS) and scanning electron microscopy combined with energy dispersive X-ray analysis (SEM/EDX).

## 1.2. Objectives of The Research

1. To study the characteristics and catalytic performances of  $\text{Bi}_x/\text{Cu}$  electrocatalysts prepared by electrodeposition of Bi on Cu foil and  $\text{Bi}_x\text{Sn}_y/\text{Cu}$  electrocatalysts prepared by electrodeposition of Bi and Sn on Cu foil with different concentration of  $\text{Bi}^{3+}$  in deposition solution for the electrochemical  $\text{CO}_2$  reduction to formate.
2. To study stability of the best catalyst that obtained the highest formate selectivity from the first objective at the appropriate potential.

## 1.3. Scopes of the Research

1. The Cu foil ( $10 \times 25 \text{ mm}^2$ ) was mechanically polished with 800G sandpaper and washed with deionized water before electrolysis.
2. The Bi/Cu electrocatalysts were prepared by electrodeposition of Bi on Cu foil ( $\text{Bi}_x/\text{Cu}$ ) or both Bi and Sn on Cu foil for  $\text{Bi}_x\text{Sn}_y/\text{Cu}$  with various concentration of  $\text{Bi}(\text{NO}_3)_3$  including 0.05 M, 0.1 M and 0.2 M. Concentration of  $\text{SnCl}_2$  kept constant

of 0.025M. The constant applied potential was set at -2.0 V. Platinum rod was used as an anode. After the deposition, the electrocatalysts were washed with DI water.

3. The catalysts performance for electrochemical CO<sub>2</sub> reduction were tested in an H-type cell at ambient condition, inlet CO<sub>2</sub> flow rate of 20 mL/min at various potential of -1.4, -1.5, -1.6, -1.7, -1.8, and -2.0 V vs. Ag/AgCl for 70 minutes. Nafion® 117 was used as a membrane separated part of the cathodic and anodic sides. Platinum foil and Ag/AgCl were used as counter electrode and reference electrode, respectively.
4. The best Bi<sub>x</sub>/Cu or Bi<sub>x</sub>Sn<sub>y</sub>/Cu catalyst that obtain the highest formate efficiency was stabilization tested at appropriate potential for 10 hours.
5. 20 mL of 0.1 M KHCO<sub>3</sub> electrolyte was filled in both cathodic side and anodic side. Before the electrolysis experiment, the electrolyte was saturated by bubbling CO<sub>2</sub> with 100 mL/min for 30 min.
6. A potentiostat was used as external power supply for electrodeposition and electrochemical reduction of CO<sub>2</sub> experiments.
7. The electrocatalysts were characterized by
  - 7.1. Scanning electron microscopy combined with energy dispersive X-ray analysis (SEM/EDX)
  - 7.2. X-ray diffraction (XRD)
  - 7.3. X-ray photoelectron spectroscopy (XPS)

## CHAPTER 2

### BACKGROUND AND LITERATUR REVIEWS

#### 2.1. Fundamental of Electrochemical CO<sub>2</sub> Reduction

The occurrence of the electrochemical CO<sub>2</sub> reduction process is shown in Fig. 1.[16] In the anode part, the oxygen evolution reaction generates electrons and protons that will be transferred to the cathode. CO<sub>2</sub> in the cathode part adopt electrons and protons and rearrange into product form.

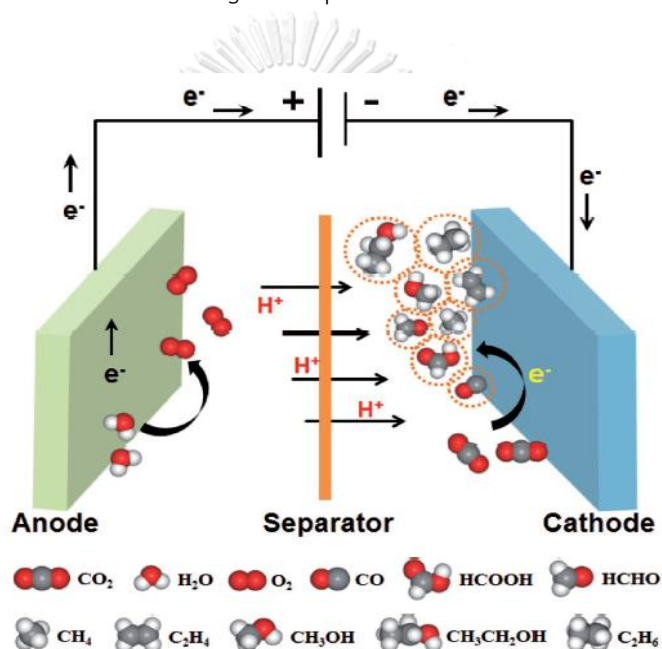
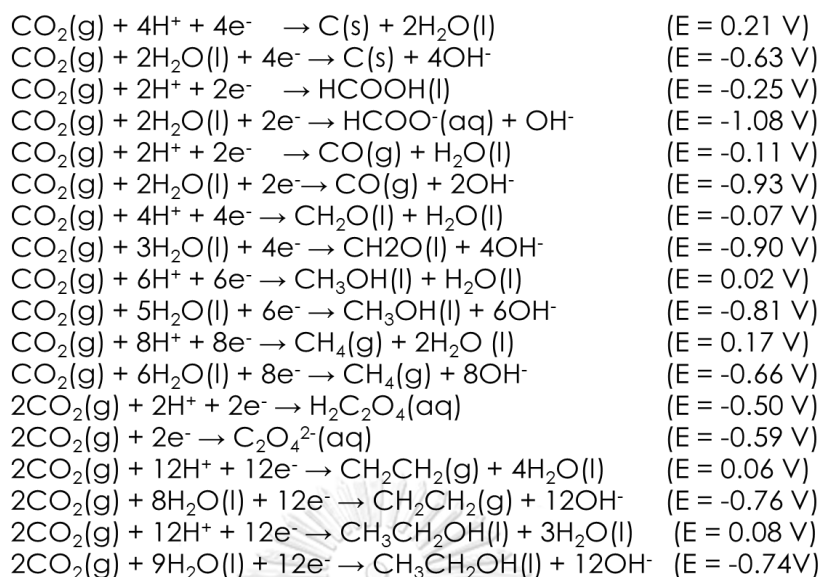


Figure 1 Schematic of the electrochemical CO<sub>2</sub> reduction process and possible products

The CO<sub>2</sub> can be reduced to various products based on the number of electrons and protons exchanged. The Half-electrochemical thermodynamic reactions and corresponding electrode potentials versus standard hydrogen electrode (SHE) in aqueous solution (at pH 7, 25 °C, 1 atm) are given below.[3]





According to the standard reduction potential, the actual applied potential often requires more negative because of single-electron reduction of  $\text{CO}_2$  to form  $\text{CO}_2^{\bullet-}$ . This step is the first step of the reduction of  $\text{CO}_2$  that extremely unfavorable due to the rearrangement of the molecule from a linear  $\text{CO}_2$  to a bent radical anion and it required as high as a negative potential of -1.97 V vs SHE.[28]

## 2.2. Study on Formate Formation on Electrodes

Electrochemical  $\text{CO}_2$  reduction reactions occur in many pathways and are produced in a variety of products. In addition to reaction conditions, applied potential, and electrolytes, catalysts play a very important role in product selection because the reaction occurs on the electrode surface. The Production of formate or formic acid from the electrochemical reduction of  $\text{CO}_2$  in an aqueous solution has been first studied in the 1870s.[16] The hydrogenation process of  $\text{H}^*$  and  $\text{CO}_2$  to produce  $^*\text{COOH}$  intermediate is the rate-determining step then the  $^*\text{COOH}$  intermediate reduced by an electron to generate formate. Afterward, various studies have demonstrated pathways of the formate formation. It was found that there are 3 main pathways including mono- or bi- dentate intermediate route,  $\text{CO}_2^{\bullet-}$  radical intermediate route, and surface-bound carbonate intermediate route as shown in Fig. 2.[2]

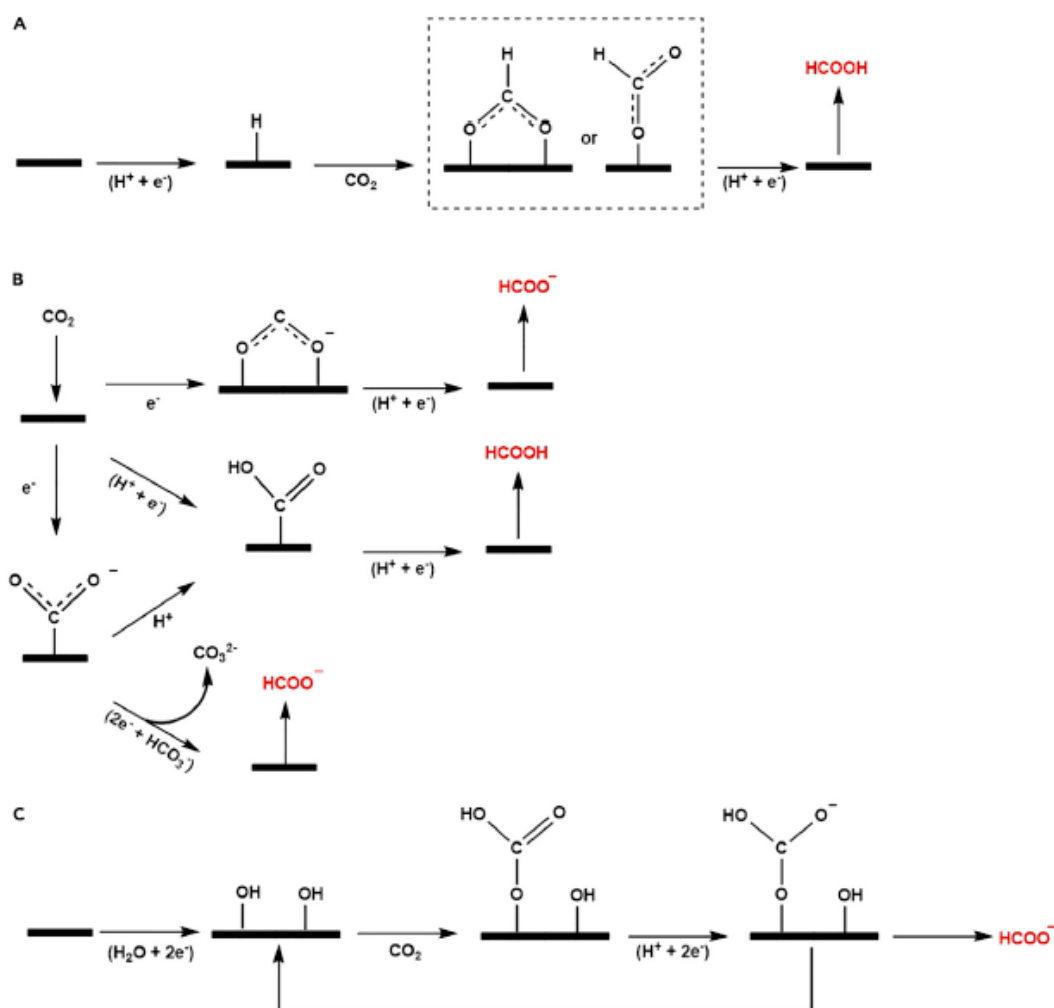


Figure 2 Mechanism for the electrochemical reduction of CO<sub>2</sub> to formate/ formic acid on metal surface. (A) mono- or bi-dentate intermediate route. (B) CO<sub>2</sub><sup>-</sup> radical route.

As shown in Fig. 2A and the top route in Fig. 2B, the intermediate formed through reaction with CO<sub>2</sub> and \*H on a metal surface into the form of monodentate or bidentate. Then formate was performed via the addition of H<sup>+</sup> and e<sup>-</sup> into the intermediate. The pathways that shown in the middle and bottom route of Fig. 2B are ascribed that CO<sub>2</sub><sup>-</sup> interact with nearby water, H<sup>+</sup> from solution or bicarbonate ions (HCO<sub>3</sub><sup>-</sup>) to generate formate. The surface-bound carbonate occurs by two electrons activated on the surface electrode and then reacts with CO<sub>2</sub> to form intermediates. This intermediate obtains electrons and a proton to form formate then desorbs to returns to the activated surface catalyst.[2]

Many researches have been studied on different types of electrocatalysts with high selectivity for formate production. There are mostly metal-based catalysts, including Pd, Pb, In, Sn, and Bi.[3],[16],[17] Table 1-5 shows summary of Pd, Pb, In, Sn, and Bi electrodes. Faradaic efficiency (FE) is the selectivity of product in terms of electrochemical.

Table 1 Pd-based electrode in electrochemical reduction of CO<sub>2</sub>

Electrode	Electrolyte	E (V vs. Ag/AgCl)	Faradaic efficiency (%)			Reference
			H <sub>2</sub>	CO	Formate	
Pd/C	0.5M KHCO <sub>3</sub>	-1.13	N/A	N/A	22	Pavesi D. et al. (2020) [29]
In <sub>95</sub> Pd <sub>5</sub> /C		-1.63	N/A	N/A	40	
mPd/TNTAs	0.5M NaHCO <sub>3</sub>	-0.77	N/A	N/A	88	Zou J. et al. (2020) [30]
PdZn NPs/CB	0.1M KHCO <sub>3</sub>	-0.71	0.4	N/A	99.4	Gunji T. et al. (2020) [31]
Pb <sub>2.25</sub> Pd <sub>3.75</sub> /CF	0.5M HCOOK	-1.50	~15	N/A	85	Lu Y. et al. (2019) [32]
Pd/CF		-0.80	~5	N/A	90	
Pd/Cu <sub>2</sub> O-Cu	0.5M NaHCO <sub>3</sub>	-0.92	<5	N/A	92	Li J. et al. (2019) [33]
Pd-B/C	0.1M KHCO <sub>3</sub>	-1.11	10	N/A	70	Jiang B. et al. (2018) [34]
Pd <sub>0.5</sub> -In <sub>0.5</sub> / 3D-RGO	0.5M KHCO <sub>3</sub>	-1.60	~10	~5	85.3	He G. et al. (2018) [35]
Pd <sub>1.0</sub> / 3D-RGO		-1.80	~10	~20	~70	
Pd Nps/C	1M KHCO <sub>3</sub>	-1.05	N/A	N/A	~100	Cai F. et al. (2017) [36]

Pd <sub>70</sub> Pt <sub>30</sub> /C	0.1M K <sub>2</sub> HPO <sub>4</sub>	-1.04	N/A	N/A	88	Kortlever R. et al. (2015) [37]
Pd-PANI/CNT	0.1M KHCO <sub>3</sub>	-0.85	N/A	N/A	83	Zhao C. et al. (2015) [38]

Table 2 Pb-based electrode in electrochemical reduction of CO<sub>2</sub>

Electrode	Electrolyte	E (V vs. Ag/AgCl)	Faradaic efficiency (%)			Reference
			H <sub>2</sub>	CO	Formate	
Pb-Sn alloy wire	0.5M KHCO <sub>3</sub>	-1.85	N/A	N/A	67.19	Widiatmoko P. et al. (2020) [39]
FD-PbNP/MWCNT/CPE	0.5M KHCO <sub>3</sub>	-1.70	~5	<3	84.6	Xing Y. et al. (2019) [40]
PbS NCs	0.1M KHCO <sub>3</sub>	-1.81	N/A	N/A	97.6	Zhang Z. et al. (2019) [41]
Pb <sub>2.25</sub> Pd <sub>3.75</sub> /CF	0.5M HCOOK	-1.50	~15	N/A	85	Lu Y. et al. (2019) [32]
Pb/CF		-1.60	~10	N/A	>80	
Pb-PhyA/CP	[Bzmim]BF <sub>4</sub>	-2.25	6.5	<2	92.7	Wu H. et al. (2018) [42]
PbO <sub>2</sub>	[Bzmim]BF <sub>4</sub>	-2.40	3.9	<2	95.5	Wu H. et al. (2018) [43]
od-Pb	Dimcarb	-1.84	11.5	11.6	80	Chen L. et al. (2017) [44]
Pb <sub>2</sub> O/(graphite plate)	0.5M KHCO <sub>3</sub>	-2.05	N/A	N/A	58.71	Yadav V. S. K. et al. (2015) [45]

Pb plate	0.1M KHCO <sub>3</sub>	-1.57	~10	N/A	88	He Z. et al. (2015) [46]
Pb-granules	0.1M K <sub>2</sub> CO <sub>3</sub>	-1.55	N/A	N/A	90	Koleli F. et al. (2003) [47]
	0.5M KHCO <sub>3</sub>	-1.85	N/A	N/A	40	

Table 3 In-based electrode in electrochemical reduction of CO<sub>2</sub>

Electrode	Electrolyte	E (V vs. Ag/AgCl)	Faradaic efficiency (%)			Reference
			H <sub>2</sub>	CO	Formate	
In/C	0.5M KHCO <sub>3</sub>	-1.63	N/A	N/A	70	Pavesi D. et al. (2020) [29]
In <sub>95</sub> Pd <sub>5</sub> /C		-1.63	N/A	N/A	40	
In-In <sub>2</sub> S <sub>3</sub>	1M KHCO <sub>3</sub>	-1.65	N/A	14	76	Yuan X. et al. (2020) [48]
Indium sheet	2mM SiW <sub>9</sub> V <sub>3</sub> - 0.1M Na <sub>2</sub> SO <sub>4</sub>	-1.60	N/A	N/A	56.82	Zha B. et al. (2020) [49]
In/Cu	0.5M KHCO <sub>3</sub>	-1.90	~25	<1	72.5	Bohlen B. et al. (2020) [50]
In-Cu/CNT	0.5M NaHCO <sub>3</sub>	-1.37	<5	19.4	84.1	Zhu M. et al. (2019) [51]
Pd <sub>0.5</sub> -In <sub>0.5</sub> / 3D- RGO	0.5M KHCO <sub>3</sub>	-1.60	~10	~5	85.3	He G. et al. (2018) [35]
In <sub>1.0</sub> / 3D- RGO		-1.60	~30	~5	~60	
In/C	0.5M NaHCO <sub>3</sub>	-2.20	N/A	N/A	94.5	Hegner R. et al. (2018) [52]

InPP/C	0.1M K <sub>2</sub> HPO <sub>4</sub>	-2.14	N/A	N/A	~60	Birdja Y. et al. (2018) [53]
MoP-In/PC	[Bmim]PF <sub>6</sub>	-2.20	<2	<2	96.5	Sun X. et al. (2018) [54]
In(OH) <sub>3</sub> /carbon black	0.5M K <sub>2</sub> SO <sub>4</sub>	-1.72	N/A	N/A	77	Rabiee A. et al. (2017) [55]
(GDE)In/C	0.1M Na <sub>2</sub> SO <sub>4</sub>	-1.65	N/A	N/A	45	Bitar Z. et al. (2016) [56]
Ag-In/Ag	0.1M KHCO <sub>3</sub>	-1.81	~15	N/A	~80	Larrazábal G. et al. (2016) [57]

Table 4 Sn-based electrode in electrochemical reduction of CO<sub>2</sub>

Electrode	Electrolyte	E (V vs. Ag/AgCl)	Faradaic efficiency (%)			Reference
			H <sub>2</sub>	CO	Formate	
SL-NG/Sn	0.5M KHCO <sub>3</sub>	-1.63	N/A	N/A	92	Huang J. et al. (2019) [58]
Pb-Sn alloy wire	0.5M KHCO <sub>3</sub>	-1.85	N/A	N/A	67.19	Widiatmoko P. et al. (2020) [39]
Sn/CC	0.1M KHCO <sub>3</sub>	-1.41	<10	~30	68.1	Lim J. et al. (2020) [59]
Nanoporous Au-Sn	0.1M KHCO <sub>3</sub>	-1.46	~10	92	<0.2	Lu X. et al. (2020) [24]
Sn/SnO <sub>x</sub>	0.1M KHCO <sub>3</sub>	-1.81	~3	~7	89.6	Lai Q. et al. (2020) [25]

Sn/CP	0.1M KHCO <sub>3</sub>	-1.70	~10	~2	88.8	An X. et al. (2019) [26]
BM Sn-Cu/Cu	0.1M KHCO <sub>3</sub>	-1.56	<10	<10	92	Jiang X. et al. (2019) [60]
SnO <sub>2</sub> /V- Al <sub>2</sub> O <sub>3</sub> /CPF	0.5M KHCO <sub>3</sub>	-2.00	N/A	N/A	75.7	Kim Y. et al. (2019) [61]
Sn metal	0.1M KHCO <sub>3</sub>	-2.01	N/A	N/A	80	Rasul S. et al. (2019) [62]
nanoporous Ag- Sn	0.5M KHCO <sub>3</sub>	-1.43	~5	~10	85	Wang X. et al (2019) [63]
np-Sn/SnO <sub>2</sub>	0.5M NaHCO <sub>3</sub>	-1.77	~10	~12	80	Liu S. et al. (2018) [64]
Sn rod	Water	-1.60	N/A	N/A	94.5	Yadav V.S.K. et al. (2018) [65]
SnS <sub>2</sub> /rGO	0.5M NaHCO <sub>3</sub>	-1.40	~17	~6	84.5	Li F. et al. (2017) [66]
Sn/f-Cu	0.1M KHCO <sub>3</sub>	-1.80	N/A	N/A	83.5	Wang Y. et al. (2016) [67]
Sn/Cu	0.1M KHCO <sub>3</sub>	-1.45	N/A	N/A	91.7	Zhao C. et al. (2016) [68]
SnO <sub>2</sub> -50/GDE	0.5M KHCO <sub>3</sub>	-1.90	N/A	N/A	56	Fu Y. et al. (2016) [69]
SnO <sub>2</sub> /N-MWCNTs	0.1M KHCO <sub>3</sub>	-1.30	N/A	N/A	46	Zhang R. et al. (2015) [70]

Sn/CP	0.45M KHCO <sub>3</sub> + 0.5M KCl	-1.40	N/A	N/A	95	Castillo D.A. et al. (2015) [71]
Sn plates	0.1M KHCO <sub>3</sub>	-1.80	N/A	N/A	85	Zhang R. et al. (2015) [72]

Table 5 Bi-based electrode in electrochemical reduction of CO<sub>2</sub>

Electrode	Electrolyte	E (V vs. Ag/AgCl)	Faradaic efficiency (%)			Reference
			H <sub>2</sub>	CO	Formate	
Bi/Cu	0.1 M KHCO <sub>3</sub>	-1.45	N/A	N/A	~100	Jiang H. et al. (2021) [73]
Bi/Ti	0.1 M KHCO <sub>3</sub>	-1.41	N/A	N/A	97	Zhao M. et al. (2020) [15]
Bi@NPC	0.1 M KHCO <sub>3</sub>	-1.55	~4	~2	92	Zhang D. et al (2020) [20]
in situ-treated Bi/Cu foam	0.1 M KHCO <sub>3</sub>	-1.60	~8	~1	92	An X. et al. (2020) [23]
Bi/Bi <sub>2</sub> O <sub>3</sub> -CP	0.5 M KHCO <sub>3</sub>	-1.50	~8	~2	90.4	Wu D. et al. (2020) [74]
Bi <sub>den</sub> /Pb	0.5 M KHCO <sub>3</sub>	-1.45	~2	N/A	98	Fan M. et al. (2020) [18]
BiOCl/C	0.5 M KHCO <sub>3</sub>	-1.50	N/A	N/A	84.3	Subramanian S. et al. (2020) [75]
Sn <sub>0.80</sub> Bi <sub>0.20</sub> alloy NPs	0.5 M KHCO <sub>3</sub>	-1.51	<2	<2	95.8	Yang Q. et al. (2020) [76]



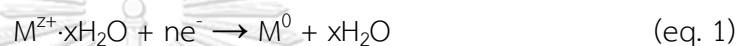
Bi-SnO/Cu foam	0.1 M KHCO <sub>3</sub>	-1.70	~5	~1	93	An X. et al. (2019) [27]
Ag-Bi-S-O	0.1 M KHCO <sub>3</sub>	-1.31	N/A	N/A	94.3	Zhou J.H. et al. (2019) [77]
Zn-Bi <sub>3</sub> /Zn	0.5 M NaHCO <sub>3</sub>	-1.47	~6	~2	94	Zhang T. et al. (2019) [9]
BiNPs/C	0.5 M KHCO <sub>3</sub>	-1.60	N/A	N/A	>93	Avila-Bolivar B. et al. (2019) [21]
Bi-GDEs/C	0.5M KCl + 0.45M KHCO <sub>3</sub>	-1.30	N/A	N/A	92.4	Díaz-Sainz G. et al. (2019) [78]
Bi/Cu	0.1 M KHCO <sub>3</sub>	-1.45	N/A	N/A	90.4	Li Q. et al. (2019) [12]
Bi-Sn/CF	0.1 M KHCO <sub>3</sub>	-1.71	~5	~2	96	Wen G. et al. (2018) [11]
SD-Bi/C	0.5 M NaHCO <sub>3</sub>	-1.42	N/A	N/A	84	Zhang Y. et al. (2018) [22]
Ultrathin Bi nanosheets/CP	0.5 M NaHCO <sub>3</sub>	-1.77	<20	<5	~110	Su P. et al. (2018) [79]
Bi <sub>m-t</sub> /CP	0.5 M KHCO <sub>3</sub>	-1.46	~12	~8	94.7	Zhang X. et al. (2018) [80]
oxide-derived Bi film/Ti	0.5 M KHCO <sub>3</sub>	-1.48	N/A	N/A	~82	Bertin E. et al. (2017) [81]
Bi/GDE	0.5 M KHCO <sub>3</sub>	-1.50	N/A	N/A	>90	Zhang X. et al. (2017) [82]

Bi-TCP	0.5 M NaHCO <sub>3</sub>	-1.85	N/A	N/A	96.4	Zhong H. et al. (2016) [19]
--------	--------------------------	-------	-----	-----	------	--------------------------------



### 2.3. Study on Electrodeposition of Bi and BiSn Electrocatalysts

Electrodeposition refers to the process of film growth, which consists of the formation of a metallic coating on a base material through the electrochemical reduction of electrolyte metal ions. [83] Electrodeposition was operated in an electrolysis cell consisting of an electrolytic bath, an anode (the positive electrode), a cathode (the negative electrode), and an external power supply. The reaction at the anode is oxidation when at the cathode is reduction. The cathode is a substrate that is deposited by metal (M). [84] The simplest case of metal ion discharge is written as equation 1 [83] :



Steps in the cathodic metals deposition in salt solutions are shown in Fig. 3. In bulk solution, the metal ions are in the form of hydrated ions  $M(H_2O)_x^{Z+}$ , where x is a number of water molecules. Hydrated ions are transferred to the cathode surface. The arrangement of the water molecules occurs in the diffusion layer then the molecules are removed in the Helmholtz layer. Ion adsorption happens on the surface of the cathode (adatoms) then the crystal lattice occurs after surface diffusion and the incorporation of adatoms. [84]

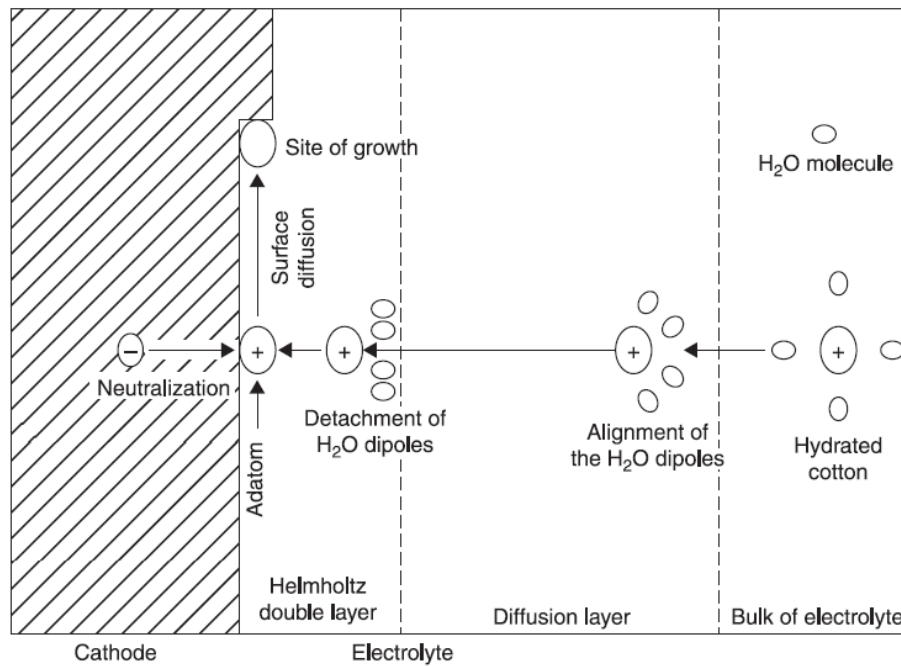


Figure 3 Schematic representation of steps in the cathodic deposition of metals.

Electrodeposition reactions take place between the cathode surface and electrolyte interfacial region. The amount of metal deposited ( $W$ ) on cathode surface is determined from the electrochemical equivalent of the metal ( $z_c$ ) and the product of quantity of total coulombs passed ( $Q_c$ ) as defined in equation 2-4. [84]

$$Q_c = \int I \, dt \quad (\text{eq. 2})$$

$$z_c = M_w / nF \quad (\text{eq. 3})$$

$$W = \int I \, dt \, M_w / nF \quad (\text{eq. 4})$$

Where  $I$  is deposition current,  $t$  is deposition times,  $M_w$  is molecular weight of metal,  $F$  is faraday constant and  $n$  is a number of exchanged electron.

Table 6-7 demonstrate the summary of Bi and BiSn electrocatalysts which is prepared by electrodeposition method.

Table 6 Bi electrodes prepared by electrodeposition

Researcher	Electrode name	Catalyst preparation	Faradaic efficiency of formate
Jiang H. et al (2021) [73]	Bi/Cu	Copper foil (2x2 cm <sup>2</sup> ) substrate was electropolished in 6 H <sub>3</sub> PO <sub>4</sub> : 2 HNO <sub>3</sub> : 3 CH <sub>3</sub> COOH solution at 3 V for 1 min. A deposition solution composed of 0.47M C <sub>7</sub> H <sub>6</sub> O <sub>6</sub> S•2H <sub>2</sub> O, 0.13M Bi(NO <sub>3</sub> ) <sub>3</sub> •5H <sub>2</sub> O, 0.27M EDTA, 0.21M Seignette salt, and 0.80M KCl. The Bi was deposited on Cu via 3 methods including constant potential of -1.0 V, direct-current of 20 mA cm <sup>-2</sup> , and pulse-current of 20 mA cm <sup>-2</sup> with frequency of 0.033 Hz. All methods were completed when the total charge reach 20 C.	100% (-1.45 V vs. Ag/AgCl)
Zhao M. et. al (2020) [15]	Bi nanosheets/Ti	Titanium sheet (1x2 cm <sup>2</sup> ) was used as electrodeposition substrate in electrolyte containing 0.025M Bi(NO <sub>3</sub> ) <sub>3</sub> •5H <sub>2</sub> O, 0.01M citric acid and 0.5M HNO <sub>3</sub> . A constant potential was applied at -0.8 V vs. Ag/AgCl for 180 s with 3 electrodes system (including Ti, Ag/AgCl and Pt mesh). Then electrocatalyst was immersed in O <sub>2</sub> -saturated 0.1M KHCO <sub>3</sub> solution for 24 h and reduced in 0.1M N <sub>2</sub> feed aqueous KHCO <sub>3</sub> at -0.8 V vs. RHE for 1 h	97% (-1.41 V vs Ag/AgCl)

An X. et al. (2020) [23]	in situ-treated Bi/Cu foam	Cu foam was immersed in the 0.05M BiCl <sub>3</sub> and 1M HCl solution at potential of -0.2V for 10 min. Then the electrode was treated at potential of -1.6 V in a CO <sub>2</sub> -sat 0.1M KHCO <sub>3</sub> for 2 h and dried in the air at 60°C for 12 h.	92% (-1.60 V vs. Ag/AgCl)
Fan M. et al. (2020) [18]	Bi <sub>den</sub> /Pb	A 0.5 cm <sup>2</sup> Pb plate was used as substrate. The electrodeposition was performed in 1mM Bi(NO <sub>3</sub> ) <sub>3</sub> and 1M HCl solution with various current densities from -0.1 to -0.4 A cm <sup>-2</sup> , and various deposition times from 1 to 40 min	98% (-1.45 V vs. Ag/AgCl)
Zhang Y. et al. (2018) [22]	SD-Bi/C	Bi <sub>2</sub> S <sub>3</sub> was synthesized by 30 mg Bi(NO <sub>3</sub> ) <sub>3</sub> ·5H <sub>2</sub> O and 70 mg thiourea and 18 mL water heated in autoclave at 200 °C for 24 h, centrifuged and dried in vacuum. The Bi <sub>2</sub> S <sub>3</sub> was dispersed in water and pipetted onto glassy carbon plate substrate. The electrode was prepared at applied potential of -0.75 V vs. RHE in CO <sub>2</sub> -sat 0.5 M NaHCO <sub>3</sub> solution.	84% (-1.42 V vs. Ag/AgCl)
Bertin E. et al. (2017) [81]	oxide-derived Bi film/Ti	Titanium foil was used as working electrode for electroplating for total deposition charge of -1.5 C. Potential was applied at 0.06 V. The solution consisted of 1 M HCl , 0.5 M KCl and 5 mM Bi <sub>2</sub> O <sub>3</sub>	82% (-1.48 V vs. Ag/AgCl)

Zhong H. et al (2016) [19]	Bi-TCP	Carbon paper substrate was pre-treated in a tube oven at 550°C for 6 h. The deposition solution containing 0.02M Bi(NO <sub>3</sub> ) <sub>3</sub> ·5H <sub>2</sub> O, 1.2M HCl, and 0.25M KBr. The deposition potential was applied at -0.35 V vs. SCE for a different time.	96.4% (-1.85 V vs. Ag/AgCl)
-------------------------------	--------	---	-----------------------------

Jiang H. et al (2021) [73] studied the hexagonal sheets of Bi electrodes by electrodeposition method. The results demonstrated that the catalyst prepared with adding KBr obtained the highest formate faradaic efficiency about 100% at -1.45 V vs. Ag/AgCl SCE. The edges and corner sites of the Bi hexagonal sheets improve local electric field intensities structure and facilitate electron transfer on the electrode. As a result, increases the catalytic activity of CO<sub>2</sub> reduction and prevents the competitive reaction.

An X. et al. (2020) [23] studied in situ morphological transformation phenomenon of Bi/Cu foam electrodes prepared by electrodeposition. The results demonstrated the highest formate faradaic efficiency 92% at -1.6 V vs. Ag/AgCl. The high FE is the result of edges or unsaturated sites of a petal-shaped Bi nanosheet structure that effectively enhances the catalytic efficiency.

Fan M. et al. (2020) [18] studied bismuth dendrites electrodes prepared by electrodeposition. The results demonstrated the highest formate faradaic efficiency 98% at -1.45 V vs. Ag/AgCl because defects and high index facets of Bi dendrites improve the catalytic activity in the CO<sub>2</sub> reduction reaction.

Zhao M. et. Al (2020) [15] studied Bi nanosheets by 3 steps electrodeposition process including the synthesis of Bi dendrites electrodes, the preparation of Bi<sub>2</sub>O<sub>2</sub>CO<sub>3</sub> (BOC) nanosheets, and the transformation of the BOC to Bi nanosheets. The results demonstrated the highest formate faradaic efficiency of 97% at -1.41 V vs. Ag/AgCl for Bi nanosheets while 81% for Bi dendrite. Since the Bi nanosheet with atom vacancies provide the electron-rich surface contributing to the stability of the intermediates for formate formation.

Zhang Y. et al. (2018) [22] studied sulfide derived-Bi (SD-Bi) electrodes prepared by electrodeposition. The results demonstrated the highest formate faradaic efficiency 84% at -1.42 V vs. Ag/AgCl. The high efficiency is the result of defect-rich Bi structure which accelerates the electrocatalysis of CO<sub>2</sub> into formate.

Bertin E. et al. (2017) [81] studied oxide-derived Bi film electrodes prepared by electrodeposition. The results showed the highest formate faradaic efficiency 82% at -1.48 V vs. Ag/AgCl. Since the catalyst has a high surface area and stable metallic Bi form.

Zhong H. et al (2016) [19] studied bismuth nanodendrites electrodes prepared by electrodeposition. The results demonstrated that the catalyst prepared with adding KBr obtained the highest formate faradaic efficiency 96.4% at -1.85 V vs. Ag/AgCl. The Br<sup>-</sup> ion in KBr acts as a capping agent to form a complex with the Bi<sup>3+</sup> that increases the absorption amount of metal ions on the substrate.

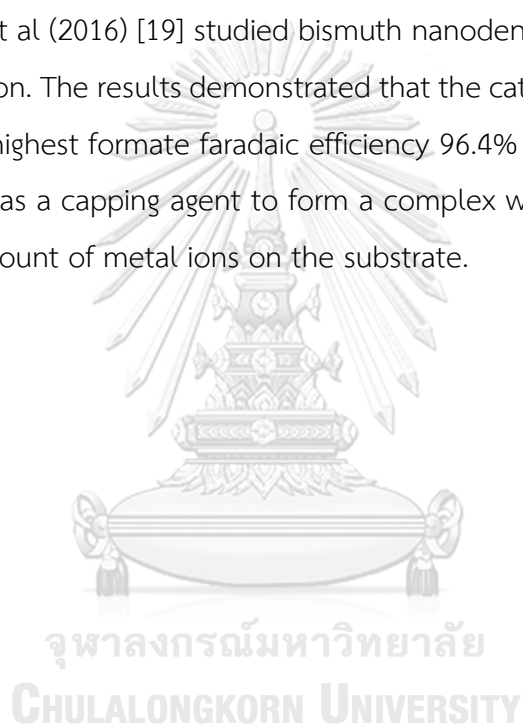




Table 7 BiSn electrodes prepared by electrodeposition

Researcher	Electrode name	Catalyst preparation	Faradaic efficiency of formate
Li Q. et al. (2019) [12]	$\text{Bi}_x\text{Sn}_y/\text{Cu}$	Copper sheet ( $1 \times 2 \text{ cm}^2$ ) was used as working electrode for electrodeposition. the solution consisted of various concentration of $\text{Bi}(\text{NO}_3)_3 \cdot 5\text{H}_2\text{O}$ , $\text{SnCl}_2 \cdot 2\text{H}_2\text{O}$ , EDTA, citric acid, and PEG 400. The electrocatalyst was fabricated with different deposition times of 20, 40, 60, and 80 min and different currents of 10, 20, 30, and 40 mA.	90.4% (-1.71 V vs. Ag/AgCl)
Wen G. et al. (2018) [11]	Bi-Sn/CFW	$\text{SnO}_2$ was grown on carbon fabrics ( $1.0 \times 1.0 \text{ cm}^2$ ) surface by hydrothermal method. The solution contains 0.5646g $\text{SnCl}_2 \cdot 2\text{H}_2\text{O}$ , 0.4508g urea, 0.1122g ammonium fluoride and DDI water then the solution was transfer to autoclave and operated at 180 °C for 10 h. The electrode was immersed Bi in Bi-solution prepared by 0.9700g $\text{Bi}(\text{NO}_3)_3 \cdot 5\text{H}_2\text{O}$ , 60ml DDI water and HCl. The electrodeposition potential was applied on -0.1 V vs. SCE. Then the electrode was conducted in $\text{CO}_2$ -saturated 0.5 m $\text{KHCO}_3$ at -1.8 V vs. SCE to reduce the $\text{SnO}_2$ to Sn.	96% (-1.45V vs. Ag/AgCl)

Li Q. et al. (2019) [12] studied  $\text{Bi}_x\text{Sn}_y$  bimetallic electrodes prepared by electrodeposition method. The concentrations of Sn, currents, and deposition times were varied. The results demonstrated that the 20 min, 30 mA Bi/Cu electrode

obtained the highest formate faradaic efficiency 90.4% at -1.71 V vs. Ag/AgCl. Increasing Bi mole content improves formate selectivity because the formation of  $\text{CHOO}^*$  intermediate favorite occurs on Bi(012) surface.

Wen G. et al. (2018) [11] studied Bi-Sn bimetallic electrodes prepared by 2 steps including hydrothermal and electrodeposition methods. The results demonstrated the highest formate faradaic efficiency 96% at -1.45 V vs. Ag/AgCl. The high efficiency is the result of the Bi-Sn interface increased the adsorption ability of the  $\text{HCOO}^*$  intermediates that favored formate production.

From the literature review, there are several electrocatalysts used for electrochemical  $\text{CO}_2$  reduction to formate, Bi and Sn obtain  $\text{FE}_{\text{formate}}$  above 80% in the potential range of -1.4 to -2.0 V vs. Ag/AgCl. Mostly high-efficiency catalysts must have a high surface area. The catalyst preparation with different conditions such as precursor, substrate, method, current, and potential, all affect the catalyst morphology and continue to affect the  $\text{FE}_{\text{formate}}$ . Most Bi has an efficiency greater than 90% because of intermediates on Bi surface that prefer formate to CO. Although Sn has good formate formation, some intermediates choose to produce CO. Bi-Sn bimetallic has also been found to improve electron transfer resulting in good  $\text{CO}_2$  reduction. However, in some studies are conflicting effects between the dominant properties of Bi and the dominant properties of Bi-Sn for formate formation. Besides, many catalysts have been studied for long-term stability. The cause of deactivation is worth studying that may occur from changing the form of catalysts.

## CHAPTER 3

### MATERIALS AND METHODS

#### 3.1. Materials

Chemicals used as precursors and electrolyte are listed in Table 8.

Table 8. Chemicals used as precursors and electrolyte

Chemicals	Formular	Suppliers
Bismuth nitrate pentahydrate (ACS reagent, $\geq 98.0\%$ )	$\text{Bi}(\text{NO}_3)_3 \cdot 5\text{H}_2\text{O}$	Sigma - Aldrich
Tin chloride (reagent grade, 98 %)	$\text{SnCl}_2$	Sigma - Aldrich
Citric acid (ACS reagent, $\geq 99.5\%$ )	$\text{C}_6\text{H}_8\text{O}_7$	Sigma - Aldrich
Nitric acid 65% (Analysis grade)	$\text{HNO}_3$	Merck Ltd
Potassium hydrogen carbonate (Analysis grade, $\geq 99.7\%$ )	$\text{KHCO}_3$	Acros Organics
Deionized water	$\text{H}_2\text{O}$	-

Metals used as electrodes in electrodeposition method and electrochemical reduction of  $\text{CO}_2$  are listed in Table 9.

Table 9 Metals used as electrodes in electrodeposition method and electrochemical reduction of CO<sub>2</sub>.

Electrodes	Suppliers
Copper foil (0.1 mm thick, 99.9999%)	Alfa Aesar
Platinum foil (0.1 mm thick, 99.997%)	Alfa Aesar
Platinum rod (Length 76 mm, Diameter 2mm)	Metrohm
Ag/AgCl reference electrode (length 12.5 cm)	Metrohm

### 3.2. Catalysts Preparation

#### 3.2.1. Preparation of copper foil

Before the electrodeposition, Cu foil (10×25 mm<sup>2</sup>) was mechanically polished with 800G sandpaper and was washed with DI water.

#### 3.2.2. Preparation of Bi<sub>x</sub>/Cu electrocatalysts

The Bi<sub>x</sub>/Cu electrocatalysts were prepared by electrodeposition method. The electrodeposition solution consisted of Bi(NO<sub>3</sub>)<sub>3</sub>·5H<sub>2</sub>O, the Bi precursor, and nitric acid with various concentrations as shown in Table 10, where x represents the concentration of Bi(NO<sub>3</sub>)<sub>3</sub>·5H<sub>2</sub>O. The Bi catalysts were deposited on a 10×10 mm<sup>2</sup> Cu foil substrate in two-electrode system and Pt rod was used as counter electrode. The electrodeposition experiment was carried out at a constant potential of -2.0 V for 1800 s. After the electrodeposition method, the electrocatalysts were washed with DI water before drying with N<sub>2</sub>.

### 3.2.3. Preparation of $\text{Bi}_x\text{Sn}_y/\text{Cu}$ electrocatalysts

The  $\text{Bi}_x\text{Sn}_y/\text{Cu}$  electrocatalysts were prepared by electrodeposition method. The electrodeposition solution consisted of  $\text{Bi}(\text{NO}_3)_3 \cdot 5\text{H}_2\text{O}$ ,  $\text{SnCl}_2$ , nitric acid and citric acid with various concentrations as shown in Table 10, where x and y represent the concentration of  $\text{Bi}(\text{NO}_3)_3 \cdot 5\text{H}_2\text{O}$  and  $\text{SnCl}_2$ , respectively.  $\text{Bi}(\text{NO}_3)_3 \cdot 5\text{H}_2\text{O}$ ,  $\text{SnCl}_2$  were used as the Bi and Sn precursors, respectively. To prevent precipitation, the solution preparation is divided into 2 parts: 1. Dissolve  $\text{Bi}(\text{NO}_3)_3 \cdot 5\text{H}_2\text{O}$  in nitric acid solution 2. Dissolve  $\text{SnCl}_2$  and citric acid with DI water. then mixed the two solutions together. The Bi and Sn were deposited on a  $10 \times 10 \text{ mm}^2$  Cu foil substrate in two-electrode system and Pt rod was used as counter electrode. The electrodeposition experiment was carried out at a constant potential of  $-2.0 \text{ V}$  for 1800 s. After the electrodeposition method, the electrocatalysts were washed with DI water before drying with  $\text{N}_2$ .

Table 10 Compositions of electrodeposition solutions for  $\text{Bi}_x/\text{Cu}$  and  $\text{Bi}_x\text{Sn}_y/\text{Cu}$  Electrodes.

Electrocatalyst	Composition of solution (mol/L)			
	$\text{Bi}(\text{NO}_3)_3 \cdot 5\text{H}_2\text{O}$	$\text{SnCl}_2$	nitric acid	citric acid
$\text{Bi}_{0.05}/\text{Cu}$	0.05	0	1.0	0
$\text{Bi}_{0.1}/\text{Cu}$	0.1	0	1.0	0
$\text{Bi}_{0.2}/\text{Cu}$	0.2	0	1.0	0
$\text{Bi}_{0.05}\text{Sn}_{0.025}/\text{Cu}$	0.05	0.025	0.5	0.3
$\text{Bi}_{0.1}\text{Sn}_{0.025}/\text{Cu}$	0.1	0.025	0.5	0.3
$\text{Bi}_{0.2}\text{Sn}_{0.025}/\text{Cu}$	0.2	0.025	0.5	0.3

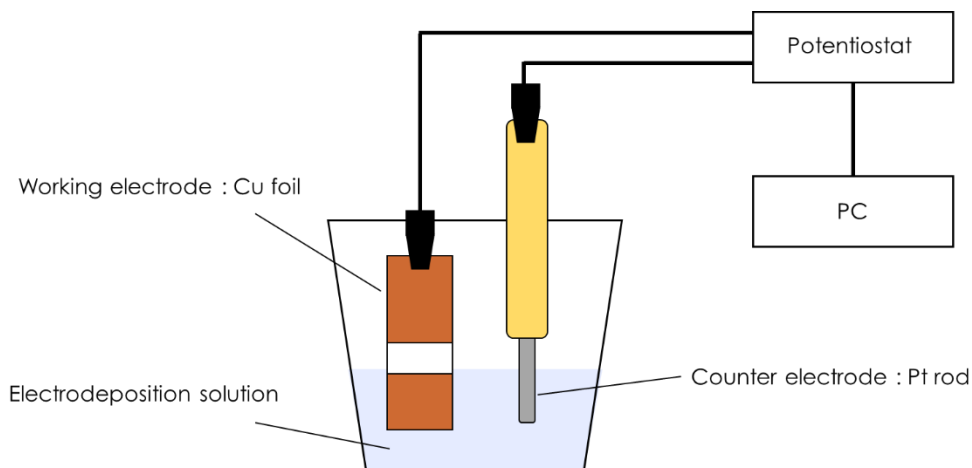


Figure 4 Schematic of preparation of  $\text{Bi}_x/\text{Cu}$  and  $\text{Bi}_x\text{Sn}_y/\text{Cu}$  electrocatalysts.

### 3.3. Catalysts Characterization

3.3.1. Scanning electron microscope combined with energy dispersive X-ray spectroscopy (SEM/EDX)

Cu foil,  $\text{Bi}_{0.05}/\text{Cu}$ ,  $\text{Bi}_{0.1}/\text{Cu}$ ,  $\text{Bi}_{0.2}/\text{Cu}$ ,  $\text{Bi}_{0.05}\text{Sn}_{0.025}/\text{Cu}$ ,  $\text{Bi}_{0.1}\text{Sn}_{0.025}/\text{Cu}$  and  $\text{Bi}_{0.2}\text{Sn}_{0.025}/\text{Cu}$  were characterized by scanning electron microscopy (SEM) of Hitachi mode S-3400N and energy dispersive X-ray spectroscopy (EDX) to investigate the morphology and element distribution on surface of catalysts.

3.3.2. X-ray photoelectron spectroscopy (XPS)

The element compositions and binding state of elements on the surface of catalysts were analyzed by AMICUS, Kratos X-ray photoelectron spectroscopy (XPS) system equipped with a nonmonochromatized Mg  $K\alpha$  X-ray source (1253.6 eV) operating at 10 kV and 20 mA.

3.3.3 X-ray diffraction (XRD)

The X-ray diffraction (XRD) pattern of electrocatalyst samples were recorded in the  $2\theta$  range  $20^\circ$ - $80^\circ$  with scan rate of 0.5 sec/step using a Siemens D5000 diffractometer and Ni filtered Cu  $K\alpha$  radiation.

### 3.4. Electrochemical Reduction of CO<sub>2</sub>

Linear sweep voltammetry (LSV) measurements were performed in an H-type cell with a three-electrode system, which consisted of the Bi<sub>x</sub>/Cu or Bi<sub>x</sub>Sn<sub>y</sub>/Cu electrode as the working electrode, a platinum counter electrode, and a Ag/AgCl reference electrode. The 0.1 M KHCO<sub>3</sub> electrolyte was bubbled with N<sub>2</sub> or CO<sub>2</sub> for 30 min to form N<sub>2</sub>-saturated or CO<sub>2</sub>-saturated solution before proceeded LSV measurements at a scan rate of 100 mV/s.

Electrochemical CO<sub>2</sub> reduction was performed in an H-type cell, and all experiments were performed at ambient condition. The cathodic and anodic side were separated by a Nafion® 117 membrane to prevent reoxidation of carbon the products at the anode. The as-prepared electrodes (Bi<sub>0.1</sub>/Cu, Bi<sub>0.05</sub>/Cu, Bi<sub>0.2</sub>/Cu, Bi<sub>0.1</sub>Sn<sub>0.025</sub>/Cu, Bi<sub>0.05</sub>Sn<sub>0.025</sub>/Cu and Bi<sub>0.2</sub>Sn<sub>0.025</sub>/Cu) acted as working electrode. A Platinum foil and Ag/AgCl in 3M KCl solution were used as a counter electrode and a reference electrode, respectively. 20 ml of 0.1M KHCO<sub>3</sub> aqueous solution was used as electrolyte in both cathodic and anodic part. Before electrolysis, the aqueous electrolyte was saturated with 100 ml/min CO<sub>2</sub> by bubbling for 30 minutes. Then, CO<sub>2</sub> was bubbled continuously with 20 ml/min in the catholyte side during reaction. The electrochemical reductions of CO<sub>2</sub> were performed by a potentiostat with constant potentials (-1.4, -1.5, -1.6, -1.7, -1.8, and -2.0 V vs Ag/AgCl) for 70 minutes. The gas chromatography (GC) system with a thermal conductivity detector (TCD) was used to analyze gaseous products (H<sub>2</sub> and CO). Liquid phase products were identified and quantified by NMR. For catalyst degradation and stability, the electrocatalyst that obtains the highest formate selectivity was studied at the appropriate potential for 10 hours.

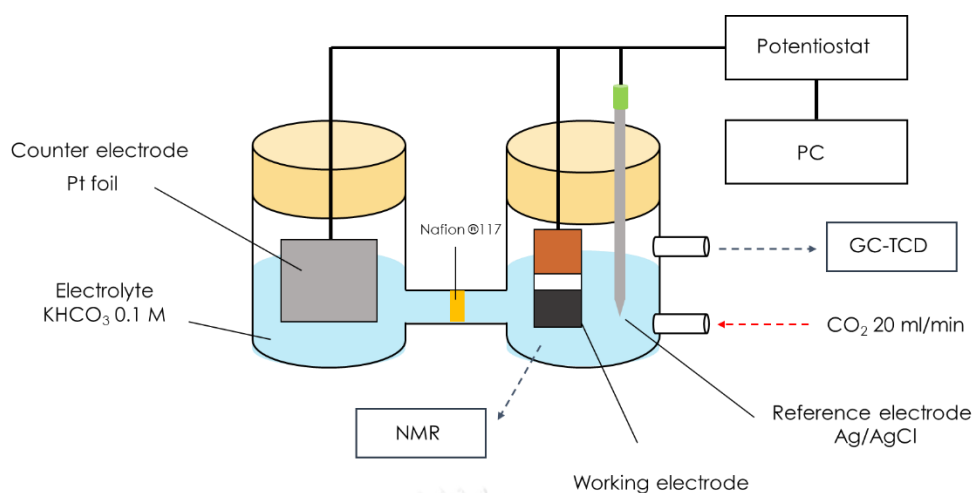


Figure 5 Schematic of electrochemical reduction of CO<sub>2</sub> system.

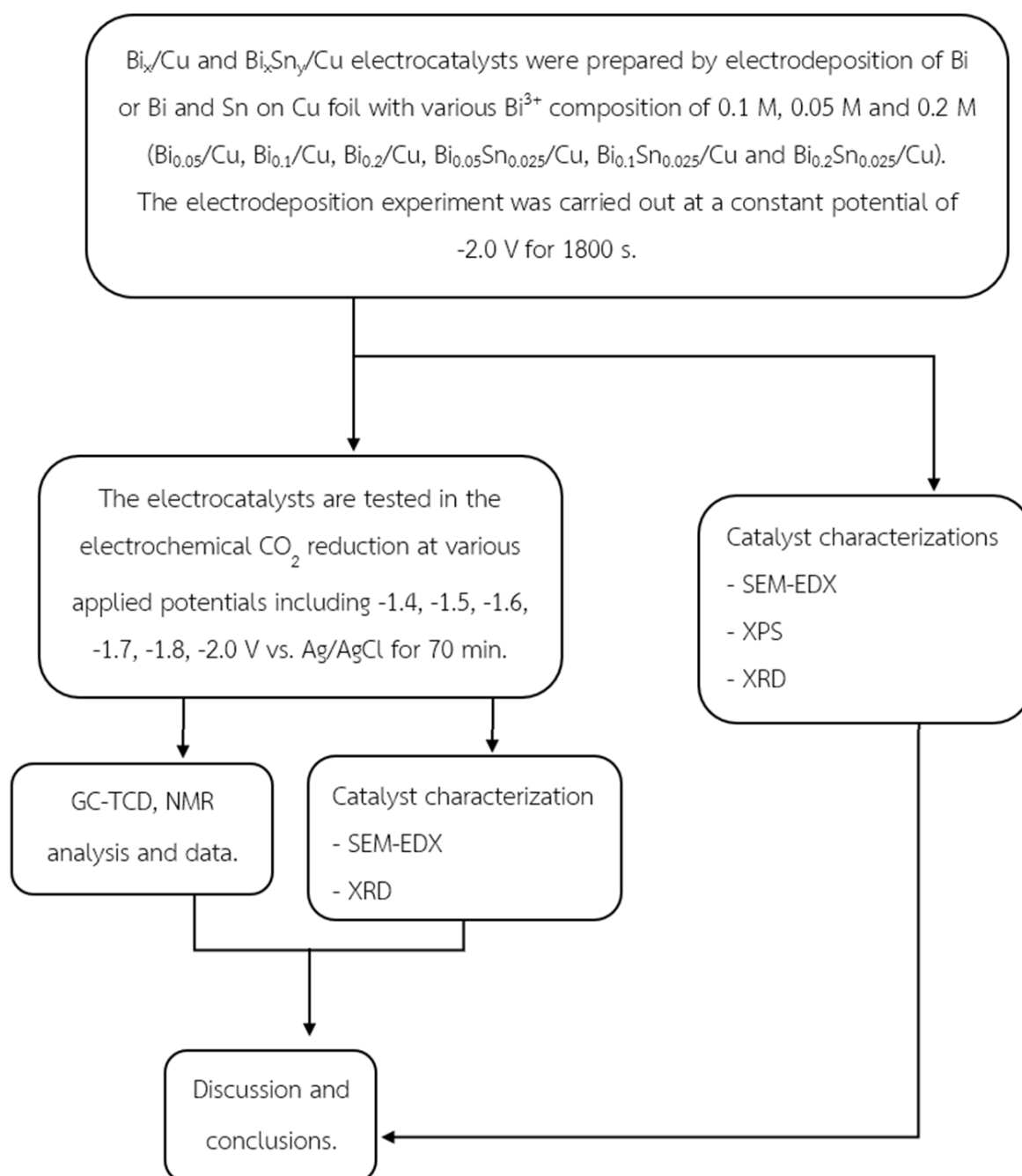
Table 11 The operating conditions of gas chromatograph with a thermal conductivity detector

Gas chromatography (Shimadzu GC-2014)	Conditions
Detector	TCD
Column type	Shincarbon ST(50/80)
Carrier gas	Helium (He: 99.999%)
Injector temperature	180°C
Column initial temperature	40°C, Hold time 5 min
Column temperature rate	10°C/min
Column final temperature	200°C
Detector temperature	170°C
Total time analysis	21 min

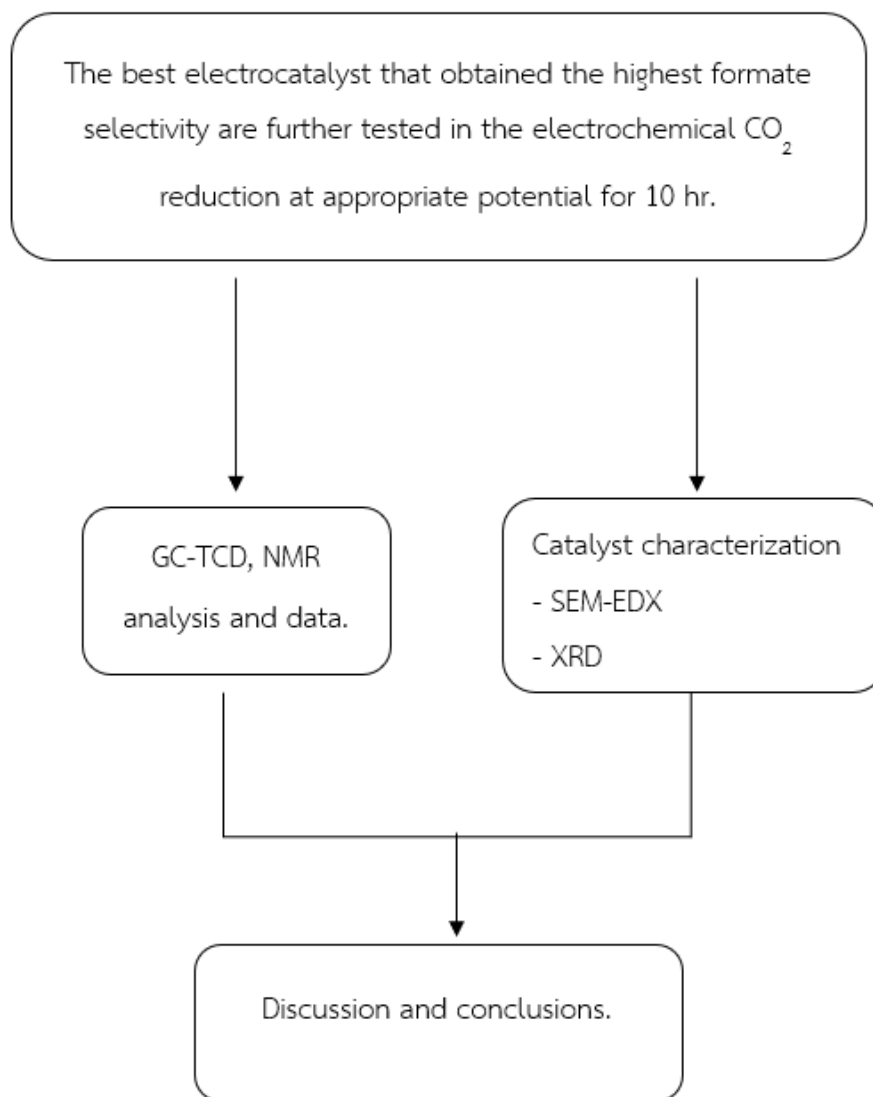


### 3.5. Research methodology

Part 1. To study the characteristics and catalytic performances of  $\text{Bi}_x/\text{Cu}$  electrocatalysts prepared by electrodeposition of Bi on Cu foil and  $\text{Bi}_x\text{Sn}_y/\text{Cu}$  electrocatalysts prepared by electrodeposition of Bi and Sn on Cu foil with different concentration of  $\text{Bi}^{3+}$  in deposition solution for the electrochemical  $\text{CO}_2$  reduction to formate.



Part 2. To study stability of the best electrocatalyst that obtained the highest formate selectivity from the first objective at the appropriate potential.



## CHAPTER 4

### RESULTS AND DISCUSSION

**Part 1.** The characteristics and catalytic performances of  $\text{Bi}_x/\text{Cu}$  electrocatalysts prepared by electrodeposition of Bi on Cu foil and  $\text{Bi}_x\text{Sn}_y/\text{Cu}$  electrocatalysts prepared by electrodeposition of Bi and Sn on Cu foil with different concentration of  $\text{Bi}^{3+}$  in deposition solution for the electrochemical  $\text{CO}_2$  reduction to formate.

#### 4.1. Characterization of $\text{Bi}_x/\text{Cu}$ and $\text{Bi}_x\text{Sn}_y/\text{Cu}$ electrocatalyst with various concentrations

4.1.1 Scanning electron microscopy combined with energy dispersive X-ray analysis (SEM/EDX)

Table 12 Weight percent and atomic percent of  $\text{Bi}_x/\text{Cu}$  and  $\text{Bi}_x\text{Sn}_y/\text{Cu}$  electrocatalysts

No	Electrocatalyst	Weight percent(%)				Atomic percent(%)			
		Bi	Sn	Cu	O	Bi	Sn	Cu	O
1	$\text{Bi}_{0.05}/\text{Cu}$	83.5	-	4.35	12.15	32.55	-	5.58	61.87
2	$\text{Bi}_{0.1}/\text{Cu}$	84.49	-	1.72	13.79	31.26	-	2.09	66.65
3	$\text{Bi}_{0.2}/\text{Cu}$	90.61	-	3.93	5.45	51.86	-	7.40	40.74
4	$\text{Bi}_{0.05}\text{Sn}_{0.025}/\text{Cu}$	94.78	0.69	1.48	3.04	67.43	0.86	3.46	28.25
5	$\text{Bi}_{0.1}\text{Sn}_{0.025}/\text{Cu}$	96.34	1.09	1.06	1.51	77.73	1.58	2.87	16.24
6	$\text{Bi}_{0.2}\text{Sn}_{0.025}/\text{Cu}$	94.42	0.42	3.65	1.51	74.41	0.58	9.46	15.54

The EDX results show surface compositions in percent by weight, as shown in Table 12. For  $\text{Bi}_x/\text{Cu}$  electrocatalysts, the percent by weight of Bi increased with increasing concentration of  $\text{Bi}^{3+}$  ion from 0.05 M to 0.2 M, whereas the Bi content on  $\text{Bi}_x\text{Sn}_y/\text{Cu}$  electrocatalysts was not significantly different and  $\text{Bi}_{0.1}\text{Sn}_{0.025}/\text{Cu}$  was slightly greater. The results of the Sn addition demonstrate that the Sn had an effect on the Bi deposited on the surface catalysts. At the same Bi concentration, the  $\text{Bi}_x\text{Sn}_y/\text{Cu}$  had

a greater percent by weight of Bi and a lower percent by weight of Cu, which is the substrate. However, because to the low concentration of  $\text{Sn}^{2+}$  in the deposition solution, a low percent by weight of Sn was detected and no substantial change in  $\text{Bi}_x\text{Sn}_y/\text{Cu}$  after electrodeposition. For atomic percent of electrodes, there are in the same trend with percent by weight. Similarly, the atomic percent of Bi in  $\text{Bi}_x/\text{Cu}$  increased after Bi concentration reached 0.2 M, while Bi and Sn atomic contents on  $\text{Bi}_x\text{Sn}_y/\text{Cu}$  had no major difference.

The SEM images of Cu foil,  $\text{Bi}_{0.05}/\text{Cu}$ ,  $\text{Bi}_{0.1}/\text{Cu}$ ,  $\text{Bi}_{0.2}/\text{Cu}$ ,  $\text{Bi}_{0.05}\text{Sn}_{0.025}/\text{Cu}$ ,  $\text{Bi}_{0.1}\text{Sn}_{0.025}/\text{Cu}$ , and  $\text{Bi}_{0.2}\text{Sn}_{0.025}/\text{Cu}$  are shown in Fig. 6. Figure 6a presents the streaky surface of Cu substrate after mechanical polishing pretreatment. Figures 6b, 6c, and 6d demonstrate the catalyst surface of  $\text{Bi}_{0.05}/\text{Cu}$ ,  $\text{Bi}_{0.1}/\text{Cu}$ , and  $\text{Bi}_{0.2}/\text{Cu}$ , respectively. It can be seen that  $\text{Bi}_{0.05}/\text{Cu}$  and  $\text{Bi}_{0.1}/\text{Cu}$  have the similar catalyst structure which is bulky structure. For  $\text{Bi}^{3+}$  ion concentrations of 0.05 and 0.1 M, the regions of the catalyst surface had suitable concentrations for the gradual formation of Bi particles. The Bi particle was aggregated to Bi bulky. The particle sizes were related to concentrations of  $\text{Bi}^{3+}$ , with lower concentrations resulting in smaller sizes because of the low concentration at the surface regions.[85],[86],[87] As a result, Bi particles exhibited less interaction force that is observed to be absent of some Bi particles on the catalyst surface. The  $\text{Bi}_{0.05}/\text{Cu}$  and  $\text{Bi}_{0.1}/\text{Cu}$  have an average bulky particle size of 8-12  $\mu\text{m}$  and 12-20  $\mu\text{m}$ , respectively. On the other hand, the  $\text{Bi}_{0.2}/\text{Cu}$  electrocatalyst from a high concentration of  $\text{Bi}^{3+}$  demonstrates the rough surface. This rough surface is caused by the tight deposition of Bi particles, due to the high concentration of  $\text{Bi}^{3+}$  at the regions of the surface, the intermolecular binding force of Bi is excessive for binding to form a bulky shape[86]. The catalyst has a significant alteration structure as can be seen from Fig. 6d. Therefore, the results show that the concentration of  $\text{Bi}^{3+}$  affects the morphology of the electrocatalysts. After adding  $\text{Sn}^{2+}$  ion in the deposition solution to fabricate  $\text{Bi}_x\text{Sn}_y/\text{Cu}$ , the rough surfaces are observed as shown in Fig. 6e, 6f, and 6g for  $\text{Bi}_{0.05}\text{Sn}_{0.025}/\text{Cu}$ ,  $\text{Bi}_{0.1}\text{Sn}_{0.025}/\text{Cu}$ , and  $\text{Bi}_{0.2}\text{Sn}_{0.025}/\text{Cu}$ , respectively. Due to the size of  $\text{Sn}^{2+}$  ion is similar to  $\text{Bi}^{3+}$  ion[88], they created a stronger interaction between the ion-molecule and the substrate causing the accumulation of catalyst particles to form a

rough surface.[89],[85],[87],[90],[91] For the Bi concentrations of 0.05 and 0.1 M, the structures of both electrodes were similar. The difference was only in the size of the particles, as seen in Fig. 6e and 6f. When increasing Bi concentration to 0.2 M, the excessive concentration affects a rough surface of  $\text{Bi}_{0.2}\text{Sn}_{0.025}/\text{Cu}$  which is different from  $\text{Bi}_{0.5}\text{Sn}_{0.025}/\text{Cu}$  and  $\text{Bi}_{0.1}\text{Sn}_{0.025}/\text{Cu}$ . As a result, the SEM images indicate that the presence of Sn and the over-concentration of Bi causes changes in structure Bi-catalyst and inhibits the formation of the Bi bulky structure.

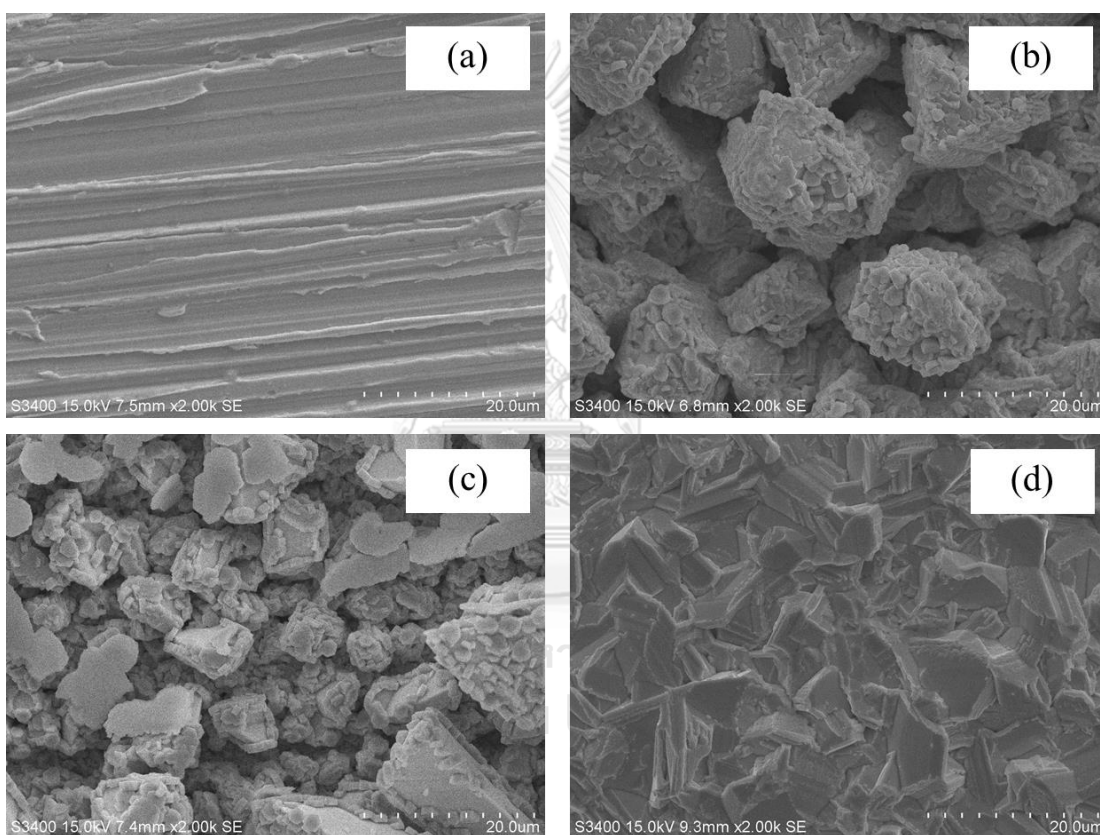


Figure 6 SEM images of (a) Cu foil, (b)  $\text{Bi}_{0.05}/\text{Cu}$ , (c)  $\text{Bi}_{0.1}/\text{Cu}$ , (d)  $\text{Bi}_{0.2}/\text{Cu}$ , (e)  $\text{Bi}_{0.05}\text{Sn}_{0.025}/\text{Cu}$ , (f)  $\text{Bi}_{0.1}\text{Sn}_{0.025}/\text{Cu}$  and (g)  $\text{Bi}_{0.2}\text{Sn}_{0.025}/\text{Cu}$

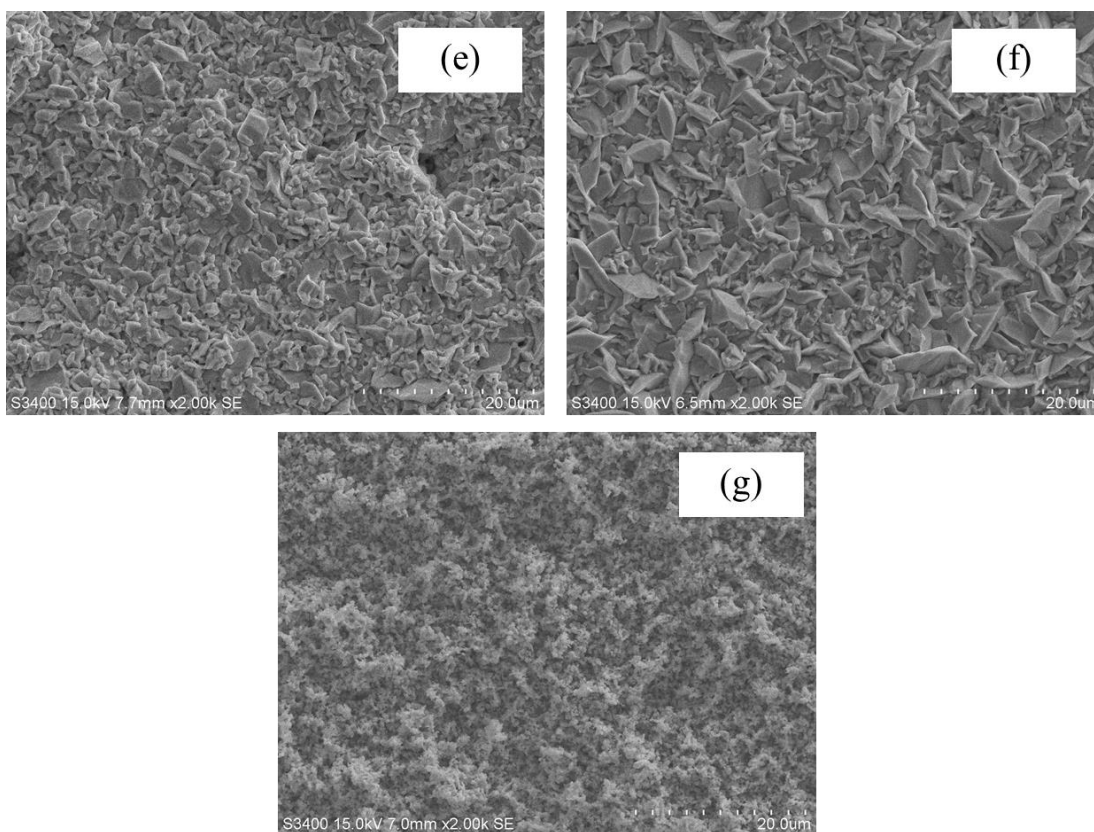


Figure 6 SEM images of (a) Cu foil, (b)  $\text{Bi}_{0.05}/\text{Cu}$ , (c)  $\text{Bi}_{0.1}/\text{Cu}$ , (d)  $\text{Bi}_{0.2}/\text{Cu}$ , (e)  $\text{Bi}_{0.05}\text{Sn}_{0.025}/\text{Cu}$ , (f)  $\text{Bi}_{0.1}\text{Sn}_{0.025}/\text{Cu}$  and (g)  $\text{Bi}_{0.2}\text{Sn}_{0.025}/\text{Cu}$

Table 13  $\text{EMF}_{\text{cell}}^0$  of electrodes

Electrode	$\text{EMF}_{\text{cell}}^0$ (V)
$\text{Bi}_x/\text{Cu}$	1.25
$\text{Bi}_x\text{Sn}_y/\text{Cu}$	1.01

In addition, adding  $\text{Sn}^{2+}$  into deposition solution results in the competitive deposition of  $\text{Bi}^{3+}$  and  $\text{Sn}^{2+}$  on Cu substrate. The electromotive force or EMF indicates the ability of current flow[92], [93]. According to Table 13,  $\text{EMF}_{\text{cell}}^0$  of  $\text{Bi}_x/\text{Cu}$  was greater than  $\text{Bi}_x\text{Sn}_y/\text{Cu}$ , indicating it easier to electrodeposit. Although the EDX results reveal that  $\text{Bi}_x\text{Sn}_y/\text{Cu}$  contained more percent by weight of Bi, the amount of Bi deposited and the active area may be less than  $\text{Bi}_x/\text{Cu}$  as seen in SEM images.

#### 4.1.2 X-ray photoelectron spectroscopy (XPS)

The surface chemical states of the electrocatalysts were investigated by X-ray photoelectron spectroscopy and the results are shown in Fig. 7 and 8. Figures 7a, 7b, and 7c demonstrate the Bi 4f spectra of Bi<sub>0.05</sub>/Cu, Bi<sub>0.1</sub>/Cu, and Bi<sub>0.2</sub>/Cu, respectively. For Bi<sub>0.1</sub>/Cu and Bi<sub>0.2</sub>/Cu, two doublets of the Bi 4f spectrum are observed. The first doublet at the higher-energy level peak located at 164.4 and 159.1 eV for Bi<sub>0.1</sub>/Cu, 164.2 and 158.9 eV for Bi<sub>0.2</sub>/Cu belonged to Bi 4f<sub>5/2</sub> and Bi 4f<sub>7/2</sub>, respectively, corresponding to Bi<sup>3+</sup> species on bismuth oxide. The second doublet located at 162.2 and 156.9 eV for Bi<sub>0.1</sub>/Cu, 162.0 and 156.6 eV for Bi<sub>0.2</sub>/Cu corresponding to Bi 4f<sub>5/2</sub> and Bi 4f<sub>7/2</sub> of metallic Bi<sup>0</sup>. The Bi 4f spectra of Bi<sub>0.05</sub>/Cu presents only Bi<sup>3+</sup> species at 164.6 and 159.3 eV. This electrode cannot detect the peak of metallic Bi<sup>0</sup> due probably to the low content of Bi. Figures 8a, 8b, and 8c present the Bi 4f spectra of Bi<sub>0.05</sub>Sn<sub>0.025</sub>/Cu, Bi<sub>0.1</sub>Sn<sub>0.025</sub>/Cu, and Bi<sub>0.2</sub>Sn<sub>0.025</sub>/Cu, respectively. All Bi<sub>x</sub>Sn<sub>y</sub>/Cu electrodes were observed only in the Bi<sup>3+</sup> region peaks. Bi 4f<sub>7/2</sub> and Bi 4f<sub>5/2</sub> peaks of Bi<sub>0.05</sub>Sn<sub>0.025</sub>/Cu located at 165.1 and 159.8 eV while Bi<sub>0.1</sub>Sn<sub>0.025</sub>/Cu and Bi<sub>0.2</sub>Sn<sub>0.025</sub>/Cu were at 164.9 and 159.6 eV, and 164.8 and 159.5 eV, respectively. The intensity of Bi<sup>3+</sup> was high, suggesting that the surface of metal Bi was easily oxidized[94]. Binding energy shifted to the lower after increasing the concentration of Bi and without adding Sn due probably to the increment in electrical conductivity on the electrocatalyst surface. As a result, Bi bulky structure may enrich electrons on the surface of the catalysts that indicates a faster electron transfer in the electrolysis reaction[73].

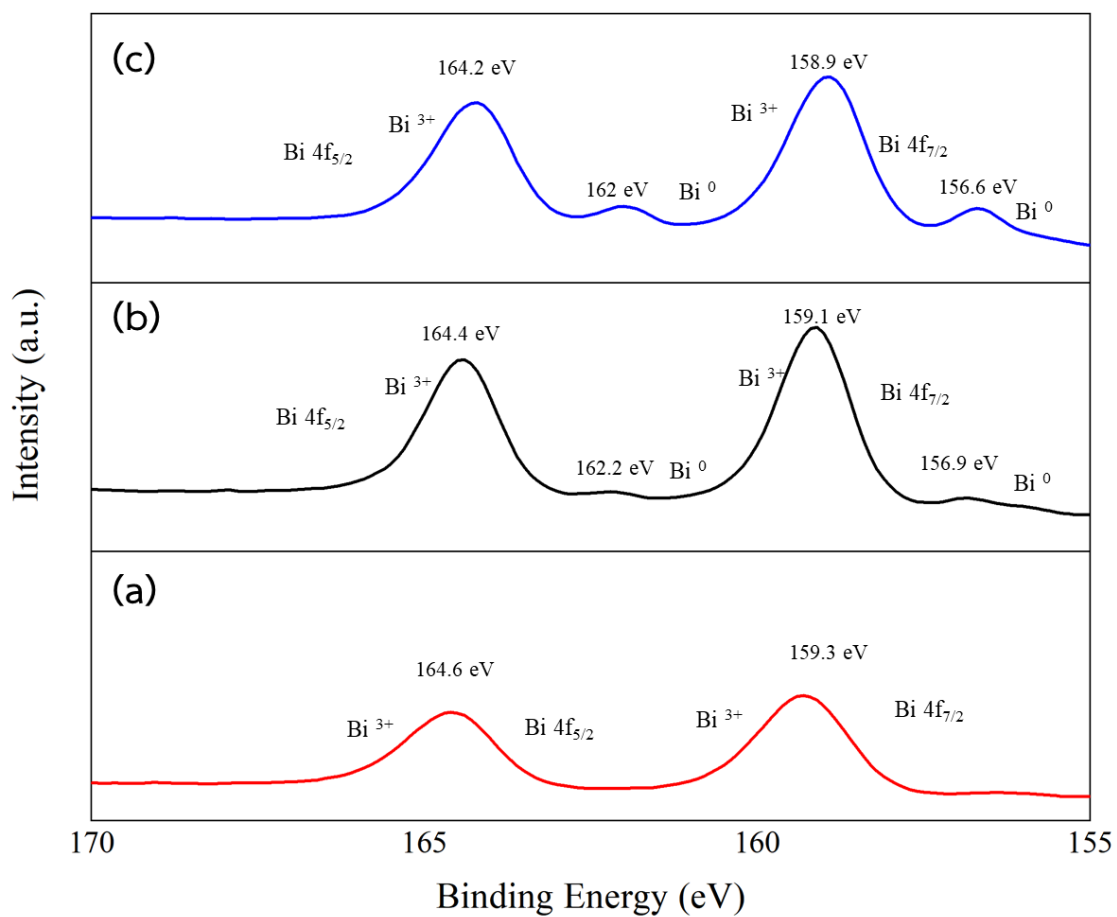


Figure 7 Bi 4f XPS spectra of (a)  $\text{Bi}_{0.05}/\text{Cu}$ , (b)  $\text{Bi}_{0.1}/\text{Cu}$ , and (c)  $\text{Bi}_{0.2}/\text{Cu}$  electrodes.



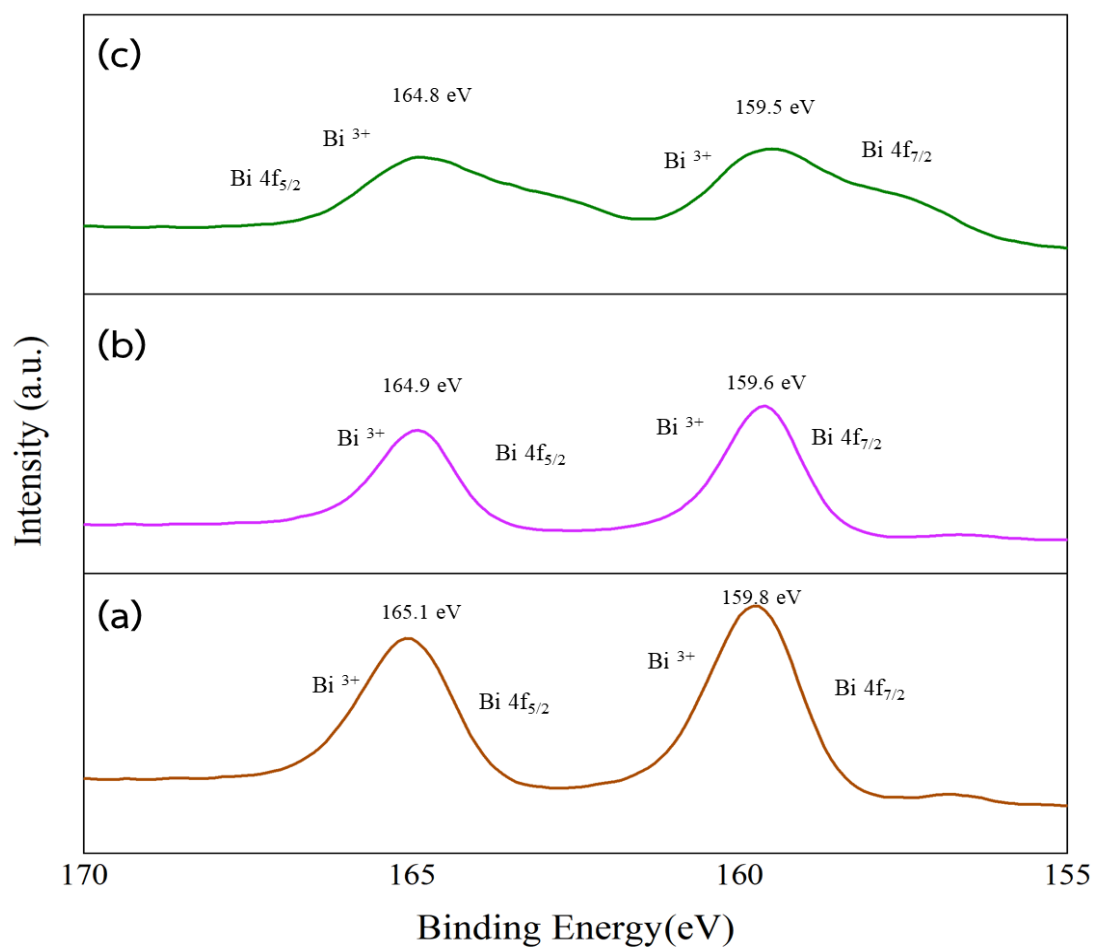


Figure 8 Bi 4f XPS spectra of (a)  $\text{Bi}_{0.05}\text{Sn}_{0.025}/\text{Cu}$ , (b)  $\text{Bi}_{0.1}\text{Sn}_{0.025}/\text{Cu}$ , and (c)  $\text{Bi}_{0.2}\text{Sn}_{0.025}/\text{Cu}$  electrodes.

#### 4.1.3 X-ray diffraction (XRD)

The crystalline structures of electrocatalysts were characterized by X-ray diffraction. Figure 9 shows XRD patterns of  $\text{Bi}_{0.05}/\text{Cu}$ ,  $\text{Bi}_{0.1}/\text{Cu}$ ,  $\text{Bi}_{0.2}/\text{Cu}$ ,  $\text{Bi}_{0.05}\text{Sn}_{0.025}/\text{Cu}$ ,  $\text{Bi}_{0.1}\text{Sn}_{0.025}/\text{Cu}$ , and  $\text{Bi}_{0.2}\text{Sn}_{0.025}/\text{Cu}$ . For  $\text{Bi}_x/\text{Cu}$ , the Bi diffraction peaks at  $23.4^\circ$ ,  $26.9^\circ$ ,  $37.7^\circ$ ,  $39.4^\circ$ ,  $44.2^\circ$ ,  $45.2^\circ$ ,  $48.5^\circ$ ,  $55.8^\circ$ ,  $62.0^\circ$ ,  $64.2^\circ$  and  $70.5^\circ$  are indexed to the (001), (012), (104), (110), (016), (113), (202), (024), (116), (112), and (214) patterns of rhombohedral Bi (JCPDS, 44-1246), respectively. The peak at  $48.5^\circ$  is the strongest following by  $26.9^\circ$  and  $39.4^\circ$ , corresponding to the (202), (012), and (110) planes, respectively. The intensity of Bi(202) and Bi(110) facets slightly increased with increasing Bi concentration from 0.05 to 0.2 M while the intensity of Bi(012) facet dropped with increasing Bi concentration from 0.05 to 0.2 M. For  $\text{Bi}_x\text{Sn}_y/\text{Cu}$ , the diffraction peaks were similar as  $\text{Bi}_x/\text{Cu}$ . A small peak at  $22.2^\circ$  was observed apart from  $\text{Bi}_x/\text{Cu}$  corresponded to Bi(003) facet. For  $\text{Bi}_x\text{Sn}_y/\text{Cu}$  electrocatalysts, the strongest peaks at  $26.9^\circ$  are indexed to (012) plane. The intensity of Bi(012) facets increased with increasing Bi concentration from 0.05 to 0.2 M. The strong diffraction peaks suggest that the Bi was highly crystalline[73]. As a result, the  $\text{Bi}_x\text{Sn}_y/\text{Cu}$  tended to grow with (012) lattice structure, whereas the Bi(202) plane was mostly fixed on  $\text{Bi}_x/\text{Cu}$  surface. Furthermore,  $\text{Bi}_{0.05}\text{Sn}_{0.025}/\text{Cu}$ ,  $\text{Bi}_{0.1}\text{Sn}_{0.025}/\text{Cu}$ , and  $\text{Bi}_{0.2}\text{Sn}_{0.025}/\text{Cu}$  present a certain amount of Sn from two small detected peaks located around  $44.0^\circ$  and  $45.1^\circ$ , corresponding to (211) and (121) facets (JCPDS 04-0673). Due to the low concentration of Sn, the XRD characteristic peaks of Sn were difficult to detect. In addition,  $\text{Bi}_{0.05}/\text{Cu}$ ,  $\text{Bi}_{0.1}/\text{Cu}$ , and  $\text{Bi}_{0.2}/\text{Cu}$  showed diffraction peaks at  $50.2^\circ$  and  $75.2^\circ$  related to Cu(200) and Cu(220) facets while  $\text{Bi}_{0.05}\text{Sn}/\text{Cu}$ ,  $\text{Bi}_{0.1}\text{Sn}_{0.025}/\text{Cu}$ , and  $\text{Bi}_{0.2}\text{Sn}_{0.025}/\text{Cu}$  were detected only (220) plane of Cu. The different results indicate the catalyst of  $\text{Bi}_x\text{Sn}_y/\text{Cu}$  covered over the entire surface of Cu rather than  $\text{Bi}_x/\text{Cu}$ .

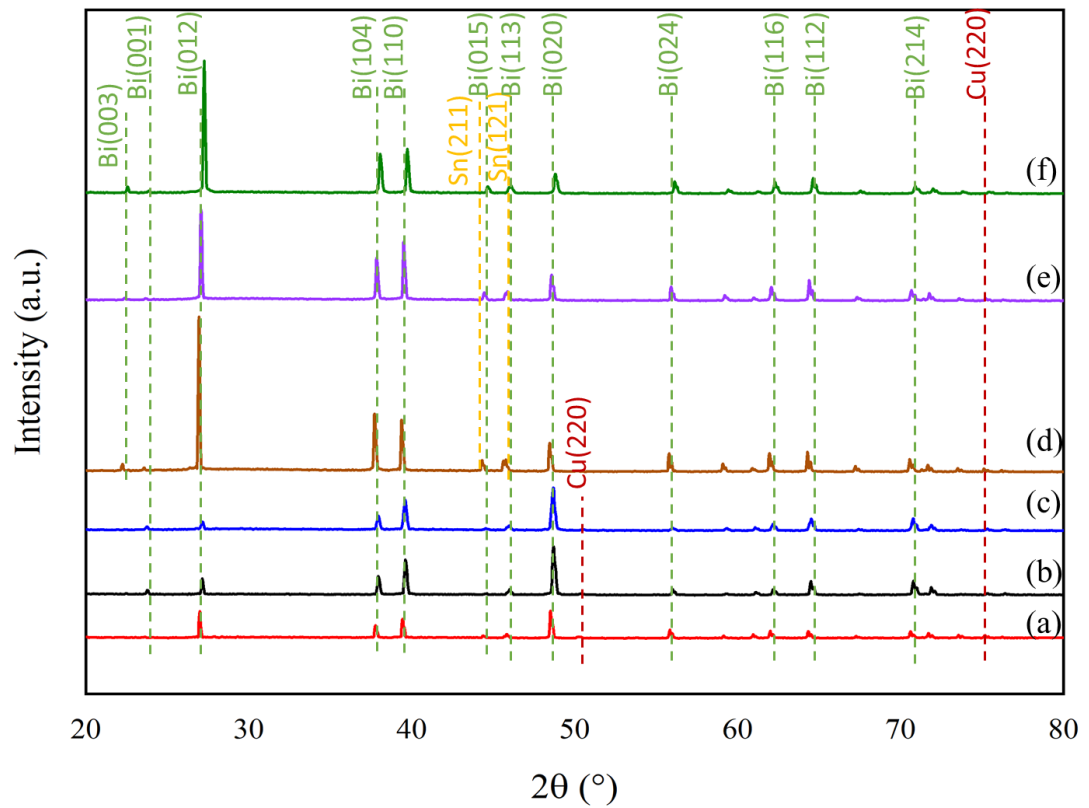


Figure 9 XRD pattern of (a)  $\text{Bi}_{0.05}/\text{Cu}$ , (b)  $\text{Bi}_{0.1}/\text{Cu}$ , (c)  $\text{Bi}_{0.2}/\text{Cu}$ , (d)  $\text{Bi}_{0.05}\text{Sn}_{0.025}/\text{Cu}$ , (e)  $\text{Bi}_{0.1}\text{Sn}_{0.025}/\text{Cu}$  and (f)  $\text{Bi}_{0.2}\text{Sn}_{0.025}/\text{Cu}$

## 4.2 Electrochemical studies

### 4.2.1 Linear sweep voltammetry test (LSV)

Table 14 the onset potential of each electrocatalyst

Electrocatalyst	Onset potential (V vs. Ag/AgCl)
Bi <sub>0.05</sub> /Cu	-1.30
Bi <sub>0.1</sub> /Cu	-1.00
Bi <sub>0.2</sub> /Cu	-1.20
Bi <sub>0.05</sub> Sn <sub>0.025</sub> /Cu	-1.35
Bi <sub>0.1</sub> Sn <sub>0.025</sub> /Cu	-1.35
Bi <sub>0.2</sub> Sn <sub>0.025</sub> /Cu	-1.30

Before electrolysis, The Performance of Bi<sub>0.05</sub>/Cu, Bi<sub>0.1</sub>/Cu, Bi<sub>0.2</sub>/Cu, Bi<sub>0.05</sub>Sn<sub>0.025</sub>/Cu, Bi<sub>0.1</sub>Sn<sub>0.025</sub>/Cu, and Bi<sub>0.2</sub>Sn<sub>0.025</sub>/Cu electrodes was first investigated to evaluate the catalytic activities by linear sweep voltammetry (LSV) test. The LSV tests were used to determine the initial potential that the reaction would occur. This applied potential is called onset potential which can be discovered when the current density begins to increase significantly. The onset potential of each electrocatalyst is shown in Table 14. Because the applied potential of -1.35 V vs. Ag/AgCl was the potential which CO<sub>2</sub> electrochemical reduction occurs for all electrodes, -1.4 V vs. Ag/AgCl was chosen as starting applied potential.

The LSV curves of all electrodes are shown in Fig. 10-15. Under N<sub>2</sub>-saturated KHCO<sub>3</sub> ascribed to the hydrogen evolution reaction (HER) are represented in dash lines. Under the CO<sub>2</sub>-saturated KHCO<sub>3</sub>, which is presented in solid line, represent the CO<sub>2</sub> reduction reaction. It can be seen that the current density of all electrocatalysts in the CO<sub>2</sub>-saturated electrolyte was higher negative than in the N<sub>2</sub>-saturated electrolyte, indicating that all Bi electrodes had a greater electrocatalytic activity for CO<sub>2</sub> reduction

reaction than hydrogen evolution reaction[15]. Compared to the different  $\text{Bi}(\text{NO}_3)_3$  concentrations of  $\text{Bi}_{0.05}/\text{Cu}$ ,  $\text{Bi}_{0.1}/\text{Cu}$ , and  $\text{Bi}_{0.2}/\text{Cu}$  electrode in the  $\text{CO}_2$ -saturated  $\text{KHCO}_3$ ,  $\text{Bi}_{0.1}/\text{Cu}$  electrode shows onset potential at  $-1.0$  V vs.  $\text{Ag}/\text{AgCl}$  then the current dramatically increased to  $-29.2$   $\text{mA}/\text{cm}^2$  at  $-1.8$  V vs.  $\text{Ag}/\text{AgCl}$ . While  $\text{Bi}_{0.05}/\text{Cu}$  and  $\text{Bi}_{0.2}/\text{Cu}$  electrode showed initial potential at  $-1.3$  and  $1.2$  V vs.  $\text{Ag}/\text{AgCl}$  and then the current rapidly increased to  $28.69$  and  $25.62$   $\text{mA}/\text{cm}^2$  at  $-1.8$  V vs.  $\text{Ag}/\text{AgCl}$ , respectively. The effect of either reducing or increasing concentrations of Bi from  $0.1$  M resulted in slightly worse catalyst performance. On the other hand, all  $\text{Bi}_x\text{Sn}_y/\text{Cu}$  electrodes showed an onset potential of about  $-1.35$  V vs.  $\text{Ag}/\text{AgCl}$  after that a current density increased to  $-21.72$ ,  $-20.30$ , and  $-18.53$   $\text{mA cm}^{-2}$  at  $-1.8$  V vs.  $\text{Ag}/\text{AgCl}$  for  $\text{Bi}_{0.05}\text{Sn}_{0.025}/\text{Cu}$ ,  $\text{Bi}_{0.1}\text{Sn}_{0.025}/\text{Cu}$ , and  $\text{Bi}_{0.2}\text{Sn}_{0.025}/\text{Cu}$  electrode, respectively. The concentrations hardly affect the elementary performances of electrocatalysts. Moreover, the  $\text{Bi}_x\text{Sn}_y/\text{Cu}$  resulted in slightly worse catalyst performance than the  $\text{Bi}_x/\text{Cu}$  since Sn doping may reduce the electrocatalyst active surface area. However, the LSV test can show only preliminary catalytic results. The electrocatalyst performances have to deeply investigate in the electrolysis of  $\text{CO}_2$ .

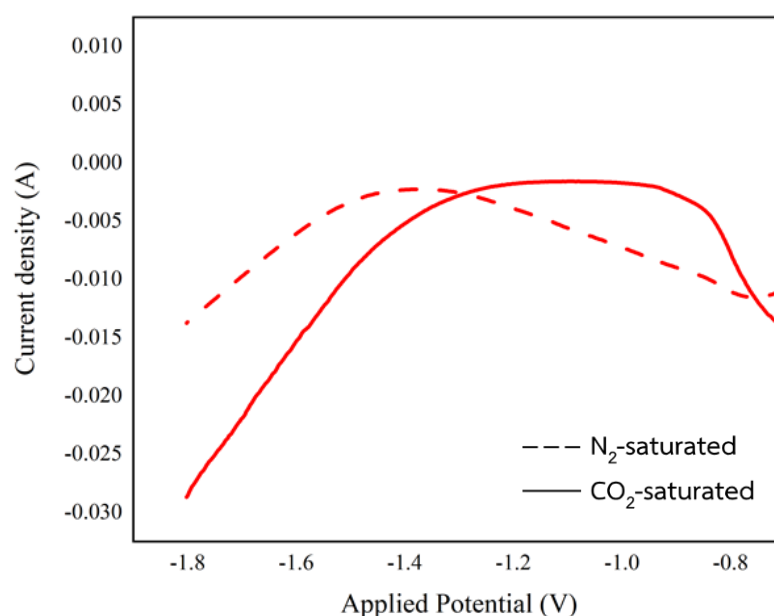


Figure 10 LSV curve of  $\text{Bi}_{0.05}/\text{Cu}$  electrode

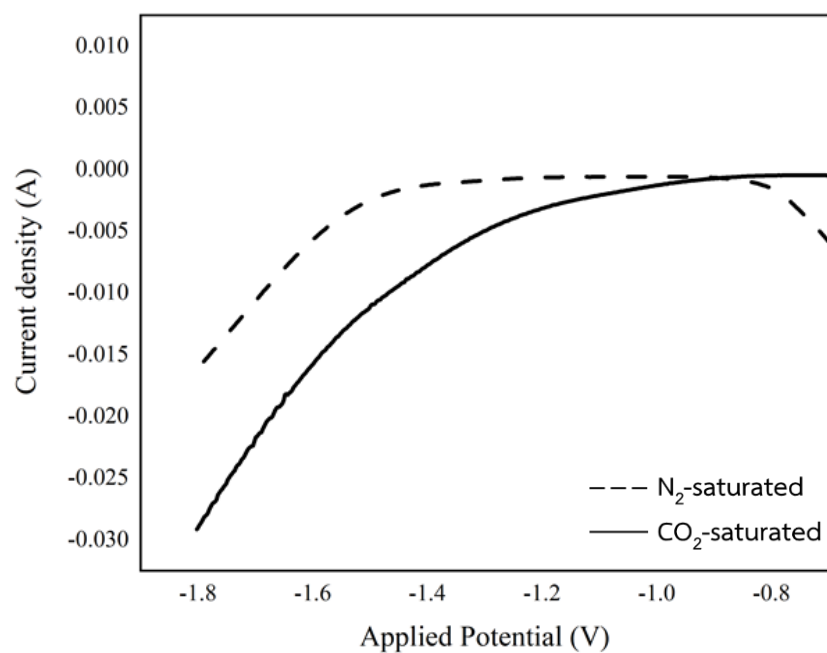


Figure 11 LSV curve of  $\text{Bi}_{0.1}/\text{Cu}$  electrode

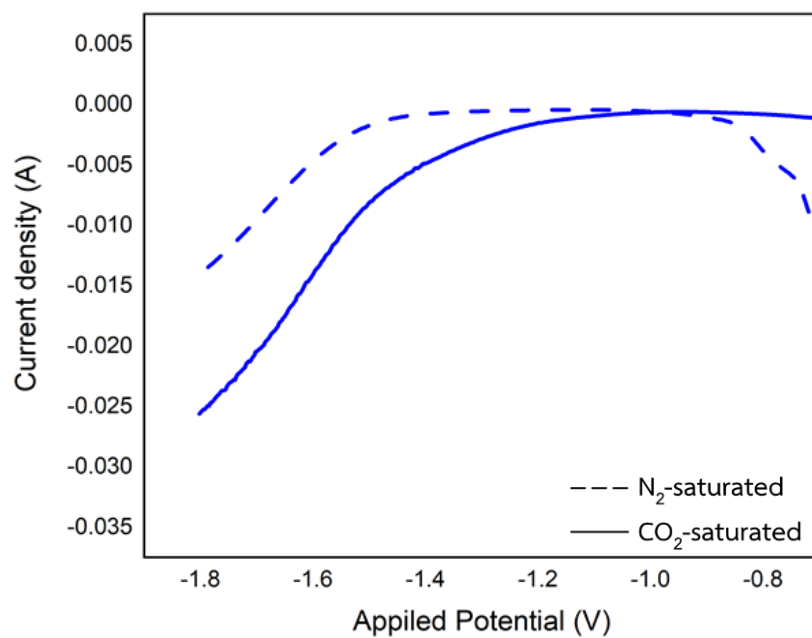


Figure 12 LSV curve of  $\text{Bi}_{0.2}/\text{Cu}$  electrode

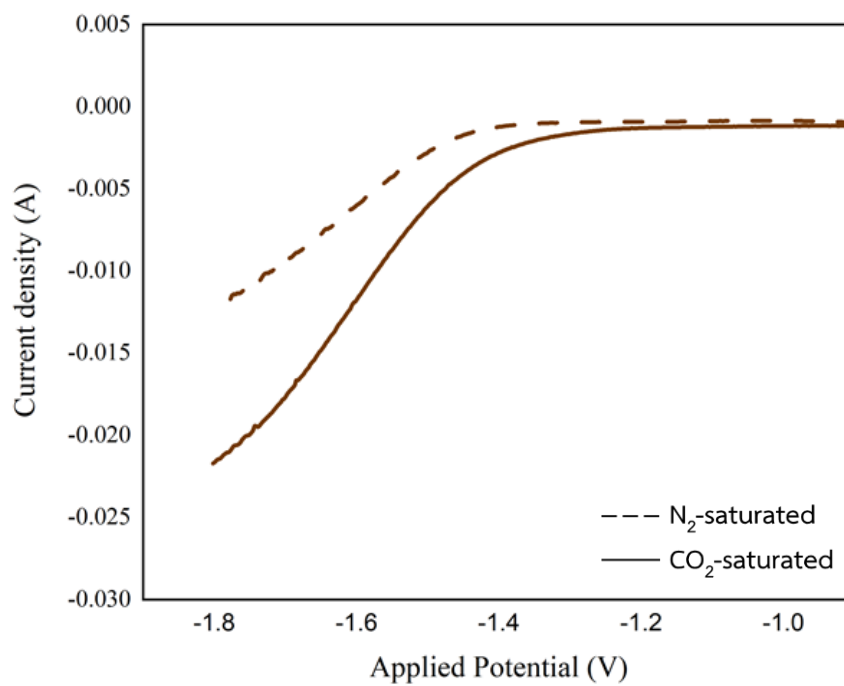


Figure 13 LSV curve of  $\text{Bi}_{0.05}\text{Sn}_{0.025}/\text{Cu}$  electrode

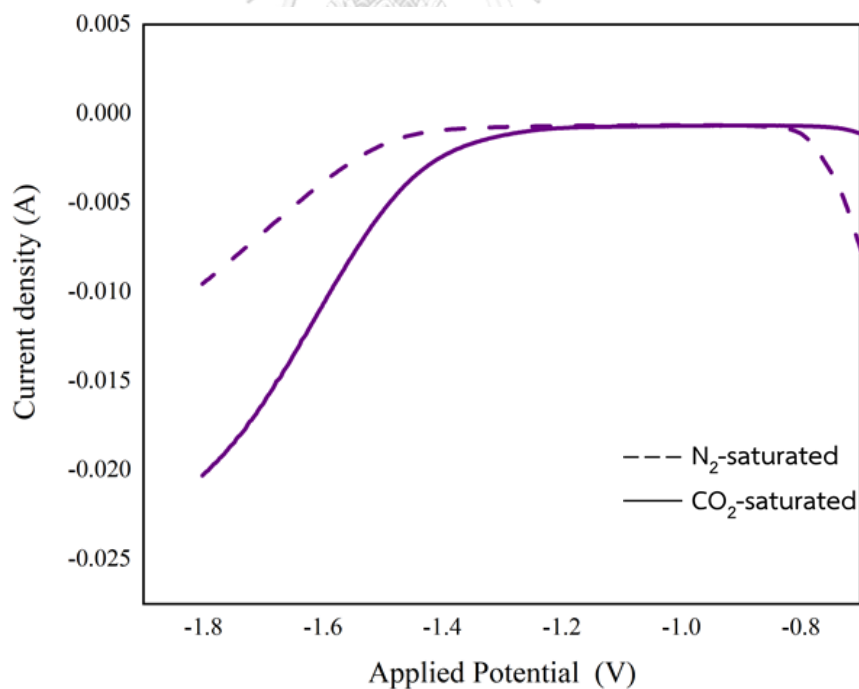


Figure 14 LSV curve of  $\text{Bi}_{0.1}\text{Sn}_{0.025}/\text{Cu}$  electrode

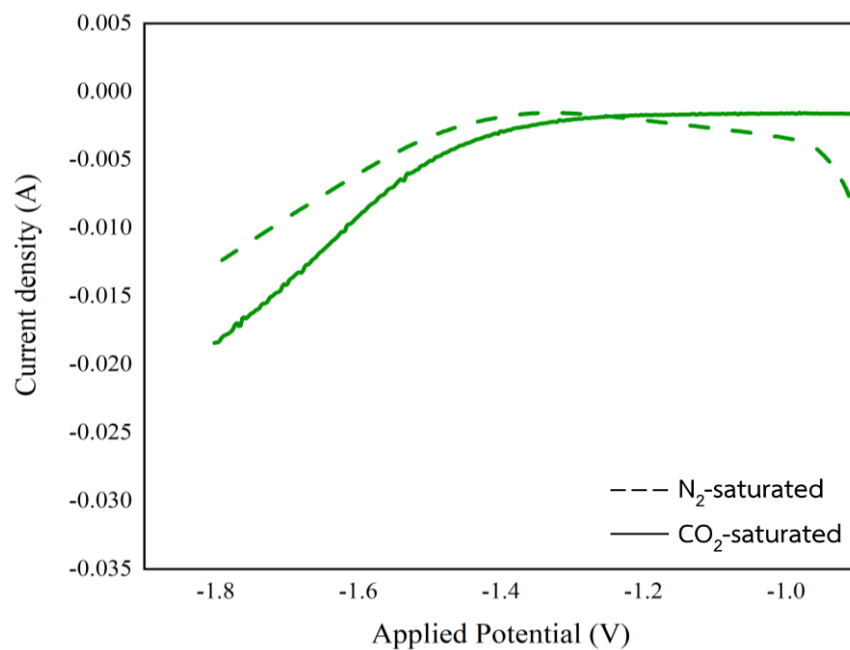


Figure 15 LSV curve of  $\text{Bi}_{0.2}\text{Sn}_{0.025}/\text{Cu}$  electrode

#### 4.2.2 Electrochemical $\text{CO}_2$ reduction test

Table 15 The catalytic performances of Cu foil, Sn foil and Bi foil

Electrode	Potential (V vs. Ag/ AgCl)	Rate ( $\mu\text{mol}/\text{min}$ )			FE Formate
		$\text{H}_2$	CO	Formate	
Cu foil	-1.40	0.0125	0.0010	0.0000	0.00
	-1.50	0.0188	0.0046	0.0076	0.62
	-1.60	0.0544	0.0083	0.2188	9.50
	-1.70	0.0673	0.0135	0.3413	9.13
	-2.00	0.2456	0.0152	0.3636	3.55
Sn foil	-1.40	0.0057	0.0033	0.0000	0.00
	-1.50	0.0118	0.0028	0.2227	18.56
	-1.60	0.0278	0.0066	0.9650	48.94
	-1.70	0.0285	0.0050	1.0253	41.57
	-1.80	0.0365	0.0038	1.2634	36.84
	-2.00	0.1170	0.0060	0.9225	11.41



Bi foil	-1.40	0.0254	0.0000	0.0390	3.94
	-1.60	0.0360	0.0006	0.4572	25.12
	-1.70	0.0301	0.0027	2.4125	61.40
	-1.80	0.0909	0.0038	3.1703	54.22
	-2.00	0.1587	0.0038	4.8933	45.98

Table 16 The catalytic performances of Bi<sub>x</sub>/Cu electrocatalysts with different Bi concentration

Electrode	Potential (V vs. Ag/ AgCl)	Rate (μmol/min)			FE Formate
		H <sub>2</sub>	CO	Formate	
Bi <sub>0.05</sub> /Cu	-1.40	0.0391	0.0000	0.0000	0.00
	-1.50	0.0250	0.0011	0.8303	43.20
	-1.60	0.0504	0.0018	1.2386	43.93
	-1.70	0.1012	0.0036	4.2950	89.34
	-1.80	0.1643	0.0042	3.7530	43.79
	-2.00	0.0913	0.0032	3.5233	40.76
Bi <sub>0.1</sub> /Cu	-1.40	0.0358	0.0004	0.0613	6.31
	-1.50	0.0452	0.0012	0.6778	33.60
	-1.60	0.0586	0.0014	1.6538	57.61
	-1.70	0.0725	0.0035	2.7848	71.42
	-1.80	0.0532	0.0037	5.4135	106.01
	-2.00	0.3390	0.0149	4.9666	51.99
Bi <sub>0.2</sub> /Cu	-1.40	0.0151	0.0002	0.2199	31.47
	-1.50	0.0527	0.0013	0.9398	39.27
	-1.60	0.0139	0.0015	1.5321	67.90
	-1.70	0.0355	0.0036	3.0270	72.57
	-1.80	0.0624	0.0048	3.6955	62.51
	-2.00	0.2187	0.0039	4.1295	39.73

Table 17 The catalytic performances of  $\text{Bi}_x\text{Sn}_y/\text{Cu}$  electrocatalysts with different Bi concentration

Electrode	Potential (V vs. Ag/ AgCl)	Rate ( $\mu\text{mol}/\text{min}$ )			FE Formate
		$\text{H}_2$	CO	Formate	
$\text{Bi}_{0.05}\text{Sn}_{0.025}/\text{Cu}$	-1.40	0.0146	0.0000	0.0000	0.00
	-1.50	0.0125	0.0005	0.5213	53.40
	-1.60	0.0172	0.0016	1.4119	80.35
	-1.70	0.0323	0.0035	2.7248	82.34
	-1.80	0.0266	0.0034	2.8480	72.64
	-2.00	0.1092	0.0040	4.4237	58.52
$\text{Bi}_{0.1}\text{Sn}_{0.025}/\text{Cu}$	-1.40	0.0111	0.0009	0.0000	0.00
	-1.50	0.0165	0.0010	0.4177	52.06
	-1.60	0.0052	0.0027	2.0977	96.87
	-1.70	0.0234	0.0038	3.5167	106.65
	-1.80	0.1043	0.0062	3.5413	69.35
	-2.00	0.2084	0.0034	4.1335	41.65
$\text{Bi}_{0.2}\text{Sn}_{0.025}/\text{Cu}$	-1.40	0.0122	0.0004	0.1732	24.98
	-1.50	0.0393	0.0012	0.4661	29.41
	-1.60	0.1066	0.0023	1.3776	31.21
	-1.70	0.0457	0.0035	2.7345	67.05
	-1.80	0.1394	0.0053	4.7652	52.09
	-2.00	0.1057	0.0062	4.8088	51.66

To investigate the electrochemical  $\text{CO}_2$  reduction performance of the electrodes on the molar flow rate of formate formation and  $\text{FE}_{\text{formate}}$ , the electrocatalysts including Cu foil, Sn foil, Bi foil,  $\text{Bi}_{0.05}/\text{Cu}$ ,  $\text{Bi}_{0.1}/\text{Cu}$ ,  $\text{Bi}_{0.2}/\text{Cu}$ ,  $\text{Bi}_{0.05}\text{Sn}_{0.025}/\text{Cu}$ ,  $\text{Bi}_{0.1}\text{Sn}_{0.025}/\text{Cu}$ , and  $\text{Bi}_{0.2}\text{Sn}_{0.025}/\text{Cu}$  were measured in the electrochemical  $\text{CO}_2$  reduction for 70 min. The electrochemical experiments were evaluated in different

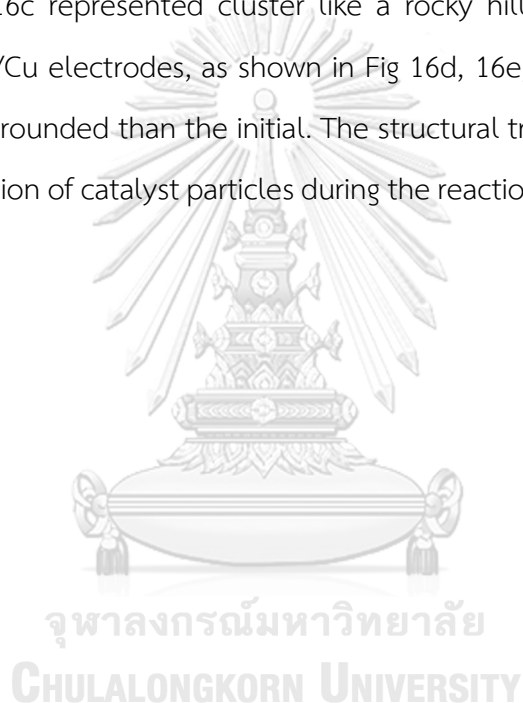
constant potentials of -1.4 to -2.0 V vs. Ag/AgCl. Table 14 shows the H<sub>2</sub>, CO, formate molar flow rate, and FE<sub>formate</sub> of Cu foil, Sn foil, and Bi foil. Cu foil exhibits the worst performance with a maximum molar flow rate of only 0.22 μmol/min with FE<sub>formate</sub> at 9.5%. Sn foil and Bi foil present higher formate production rates and FE<sub>formate</sub> than Cu foil because Cu is in group 3 of metallic electrocatalyst that is nonspecific to formate formation[28]. The formate rates of Sn foil were slightly lower than Bi foil, whereas the CO rates were quite higher. Due to the different intermediates formed during the reaction, Sn has intermediates pathways in both CO<sub>2</sub><sup>-</sup> radical and \*OOCH that can produce CO<sub>2</sub> and formate while Bi is more specific to the \*OOCH[2].

Table 15 and Table 16 present the H<sub>2</sub>, CO, formate molar flow rate, and FE<sub>formate</sub> of Bi<sub>x</sub>/Cu and Bi<sub>x</sub>Sn<sub>y</sub>/Cu. H<sub>2</sub> formation rates on Bi<sub>x</sub>Sn<sub>y</sub>/Cu electrodes are usually observed to be lower than Bi<sub>x</sub>/Cu. The presence of Sn particles on the catalyst led to the decrease of side reaction because the theoretical limiting potentials for HER is relatively high[95]. For Bi<sub>x</sub>/Cu, the formate and CO on Bi<sub>0.05</sub>/Cu could not be detected at -1.4V vs. Ag/AgCl, demonstrating that no CO<sub>2</sub> reduction occurred. After increasing applied potential, Bi<sub>0.05</sub>/Cu obtained the highest FE<sub>formate</sub> of about 89% and formate molar flow rate of 4.30 μmol/min. Meanwhile, the formate on Bi<sub>0.1</sub>/Cu and Bi<sub>0.2</sub>/Cu electrodes were first apparent at -1.4 V vs. Ag/AgCl. With increasing overpotential, the formate faradaic efficiency was rapidly increased, reaching a maximum of 106% at -1.8 V vs. Ag/AgCl with a formate molar flow rate of 5.41 μmol/min for Bi<sub>0.1</sub>/Cu electrode, and 72.6% at -1.7 V vs. Ag/AgCl with a rate of 3.02 μmol/min for Bi<sub>0.2</sub>/Cu electrode. The maximum formate rate and FE<sub>formate</sub> of Bi<sub>0.05</sub>/Cu electrode were relatively low compared to Bi<sub>0.1</sub>/Cu, resulting from smaller bulky sizes, as shown in SEM images (Fig. 6). Moreover, the decrease of formate formation on Bi<sub>0.2</sub>/Cu electrode was attributable to reduced surface area due to structural changes after increased Bi concentration of electrode. In part of Bi<sub>x</sub>Sn<sub>y</sub>/Cu, the formate rate and FE<sub>formate</sub> of Bi<sub>x</sub>Sn<sub>y</sub>/Cu were in line with Bi<sub>x</sub>/Cu. From -1.4 V vs. Ag/AgCl, Bi<sub>0.05</sub>Sn<sub>0.025</sub>/Cu and Bi<sub>0.1</sub>Sn<sub>0.025</sub>/Cu electrodes could not detect formate in the liquid product, but a small amount of CO was still detectable

on the  $\text{Bi}_{0.1}\text{Sn}_{0.025}/\text{Cu}$  electrode, demonstrating more electrocatalyst efficiency from a higher amount of Bi. With increasing applied potential,  $\text{FE}_{\text{formate}}$  reached the maximum of 82%, 106%, and 67% with rates of 2.72, 3.52, and 2.73  $\mu\text{mol}/\text{min}$  for  $\text{Bi}_{0.05}\text{Sn}_{0.025}/\text{Cu}$ ,  $\text{Bi}_{0.1}\text{Sn}_{0.025}/\text{Cu}$ , and  $\text{Bi}_{0.2}\text{Sn}_{0.025}/\text{Cu}$ , respectively. As a consequence, the influence of concentrations expressed in catalytic structures either change in size or morphology affects formate formation. Compared between before and after adding Sn, Sn-containing electrodes had similar  $\text{FE}_{\text{formate}}$  to  $\text{Bi}_x/\text{Cu}$  electrodes. For Bi concentration of 0.01 M, the maximum FE on both electrodes was equal. However, the formate molar flow rate of the  $\text{Bi}_{0.1}\text{Sn}_{0.025}/\text{Cu}$  electrode was less than the  $\text{Bi}_{0.1}/\text{Cu}$  electrode due probably to less surface area between a rough surface and bulky structure. From the high formate formation, the (202) plane of Bi on Bi-bulky structures can promote \*OOCH intermediate to the production of formate as well as Bi(012) plane on electrochemical  $\text{CO}_2$  reduction activity[80]. In addition, after electrocatalysts obtained a maximum  $\text{FE}_{\text{formate}}$  at an appropriate potential,  $\text{FE}_{\text{formate}}$  was decreased slightly after this point. It was suggested to mass transport limitations of  $\text{CO}_2$ [11]. At higher overpotential, the proton and electron pair transfer faster while  $\text{CO}_2$  transfers with the same rate resulting in HER dramatically increased, which causes  $\text{H}_2$  formation[96]. Among the study of deposited electrocatalysts,  $\text{Bi}_{0.1}/\text{Cu}$  is the best electrocatalyst that obtained the highest formate production rate of 5.41  $\mu\text{mol}/\text{min}$  and  $\text{FE}_{\text{formate}}$  of about 106% because the bulky structure of  $\text{Bi}_{0.1}/\text{Cu}$  has a higher active site and surface area. As a result,  $\text{Bi}_{0.1}/\text{Cu}$  was selected for a future study in part 2 at a potential of -1.8 V vs. Ag/AgCl.

#### 4.2.3 Scanning electron microscopy (SEM) of electrocatalysts after reaction for 70 min.

The SEM images of electrodes after electrolysis are shown in Fig 16. The results demonstrate that the morphology of electrocatalysts had rather changed compared to their structure before electrolysis (Fig. 6). For  $\text{Bi}_x/\text{Cu}$ , bulky structures of  $\text{Bi}_{0.05}/\text{Cu}$  and  $\text{Bi}_{0.1}/\text{Cu}$  in Fig. 16a and 16b decomposed into lighter clusters, which  $\text{Bi}_{0.05}/\text{Cu}$  electrode expressed cauliflower-like structure with a particle size of 4-6.4  $\mu\text{m}$  and  $\text{Bi}_{0.1}/\text{Cu}$  electrode showed clump of Bi particles with a clump sizes of 16-24  $\mu\text{m}$ , while  $\text{Bi}_{0.2}/\text{Cu}$  electrode in Fig. 16c represented cluster like a rocky hill. On the other hand, the structure of  $\text{Bi}_x\text{Sn}_y/\text{Cu}$  electrodes, as shown in Fig 16d, 16e, and 16f, retained a rough texture with more rounded than the initial. The structural transformations are perhaps caused by the erosion of catalyst particles during the reaction or the change in catalytic composition[80].



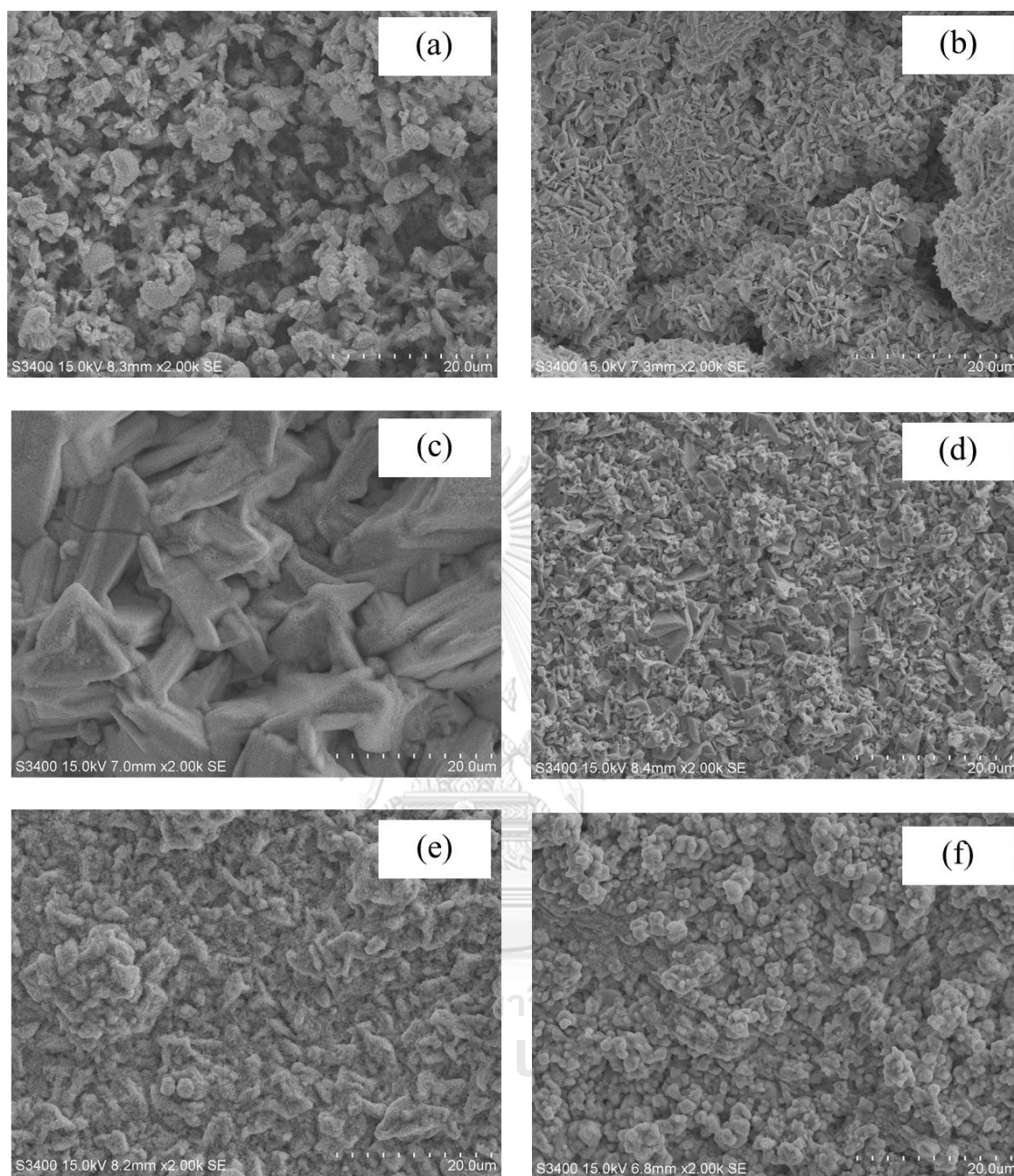


Figure 16 SEM images of (a)  $\text{Bi}_{0.05}/\text{Cu}$ , (b)  $\text{Bi}_{0.1}/\text{Cu}$ , (c)  $\text{Bi}_{0.2}/\text{Cu}$ , (d)  $\text{Bi}_{0.05}\text{Sn}_{0.025}/\text{Cu}$ , (e)  $\text{Bi}_{0.1}\text{Sn}_{0.025}/\text{Cu}$  and (f)  $\text{Bi}_{0.2}\text{Sn}_{0.025}/\text{Cu}$  after reaction

#### 4.2.4 X-ray diffraction (XRD) of electrocatalysts after reaction

The chemical compositions of electrocatalysts after the experiment were analyzed by XRD, and the results are shown in Fig 17. The new diffraction peaks appeared after reaction in the XRD pattern compared to the unused electrode. These peaks are located at 23.9°, 30.0°, 32.7°, 42.3°, and 56.9°, corresponding to (011), (013), (110), (114), and (123) facets tetragonal  $\text{Bi}_2\text{O}_2\text{CO}_3$  (JCPDS 41-1488)[23]. The appearance of these new peaks represents the formation of  $\text{Bi}_2\text{O}_2\text{CO}_3$  during the reaction leading to the changes in catalyst morphology[80].

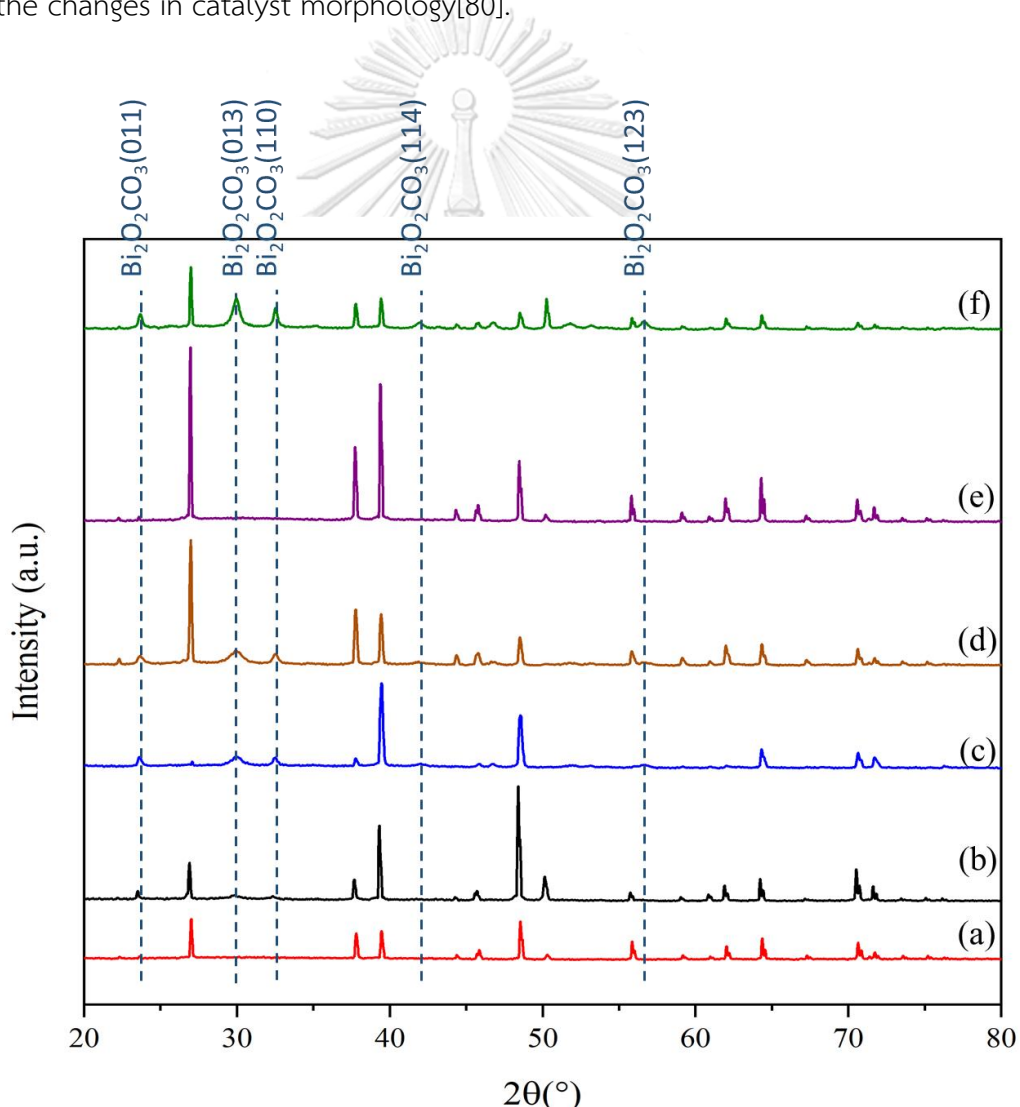


Figure 17 XRD pattern of (a)  $\text{Bi}_{0.05}/\text{Cu}$ , (b)  $\text{Bi}_{0.1}/\text{Cu}$ , (c)  $\text{Bi}_{0.2}/\text{Cu}$ , (d)  $\text{Bi}_{0.05}\text{Sn}_{0.025}/\text{Cu}$ , (e)  $\text{Bi}_{0.1}\text{Sn}_{0.025}/\text{Cu}$  and (f)  $\text{Bi}_{0.2}\text{Sn}_{0.025}/\text{Cu}$  after reaction

**Part 2.** The stability of the best electrocatalyst that obtained the highest formate selectivity from the first objective at the appropriate potential.

### 4.3 Stability test of Bi<sub>0.1</sub>/Cu in the electrochemical CO<sub>2</sub> reduction

4.3.1 The catalytic performances of Bi<sub>0.1</sub>/Cu electrode in the electrochemical CO<sub>2</sub> reduction at -1.8 V vs. Ag/AgCl for 10 hours

Table 18 The stability performances of Bi<sub>0.1</sub>/Cu

Collected time (h.)	Rate (μmol/min)			FE Formate
	H <sub>2</sub>	CO	Formate	
1	0.0532	0.0037	5.41	106.01
2	0.0846	0.0064	5.97	97.80
3	0.0879	0.0067	5.71	97.68
4	0.1132	0.0070	6.14	95.27
5	0.1000	0.0062	4.93	84.39
6	0.0912	0.0068	4.98	80.88
7	0.0967	0.0070	5.12	83.49
8	0.1170	0.0066	6.45	96.33
9	0.1252	0.0068	6.54	93.40
10	0.1280	0.0071	5.55	82.17

The stability study has been carried out on Bi<sub>0.1</sub>/Cu electrode. The stability experiment was conducted at a constant potential of -1.8 V vs. Ag/AgCl for 10 hours in CO<sub>2</sub>-saturated 0.1 M KHCO<sub>3</sub>. The electrolyte was refreshed every hour to decrease the effects of pH variations in the electrolyte from the accumulation of CO<sub>2</sub> and formate. Table 18 shows FE<sub>formate</sub> and molar flow rate of H<sub>2</sub>, CO, and formate. The formate faradaic efficiency slightly fluctuated and declined from the initial. The FE<sub>formate</sub> maintained above 80% over the experiments with an average formate production rate of 5.68 μmol/min. Moreover, H<sub>2</sub> production lightly increased with time owing to the morphology changes of the electrocatalyst or the presence of Cu substrate on the surfaces. The current density and FE<sub>formate</sub> over 10 hours are displayed



in Fig. 18. During the first hour, the current density remained relatively constant but after 10 hours, it was slightly negative increased to  $-28.45 \text{ mA/cm}^2$ .

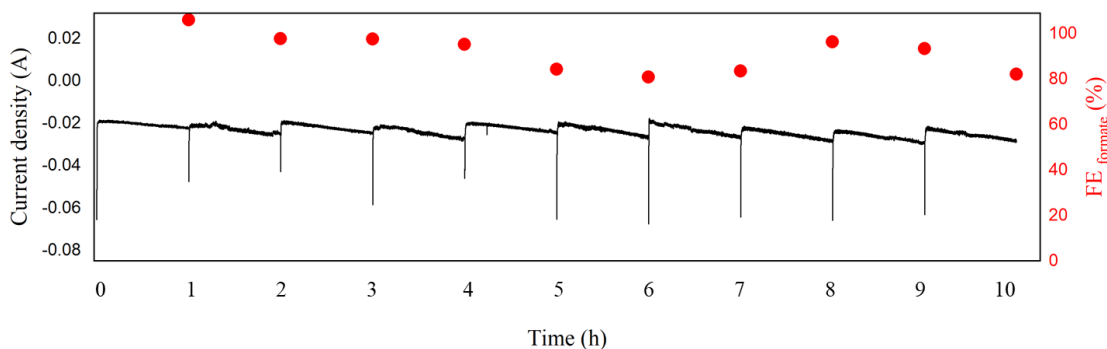


Figure 18 Current density and  $FE_{\text{formate}}$  during stability test

#### 4.3.2 Scanning electron microscopy (SEM) of electrocatalysts after stability test reaction

The morphology of  $\text{Bi}_{0.1}/\text{Cu}$  was analyzed by the scanning electron microscopy. The SEM images of electrocatalyst are displayed in Fig. 19a and 19b correspondingly before and after the stability experiment. The morphology of  $\text{Bi}_{0.1}/\text{Cu}$  has slightly changed compared to the initial. Before the stability experiment, Bi bulky had a particles size of  $12\text{-}20 \mu\text{m}$ . The particle size of Bi bulky after the stability test was  $16\text{-}25.6 \mu\text{m}$  which are larger than  $\text{Bi}_{0.1}/\text{Cu}$  before the stability test. The increase of Bi bulky sizes is presumably due to the agglomeration of Bi particles and the formation of  $\text{Bi}_2\text{O}_2\text{CO}_3$  during the electrolysis[80].

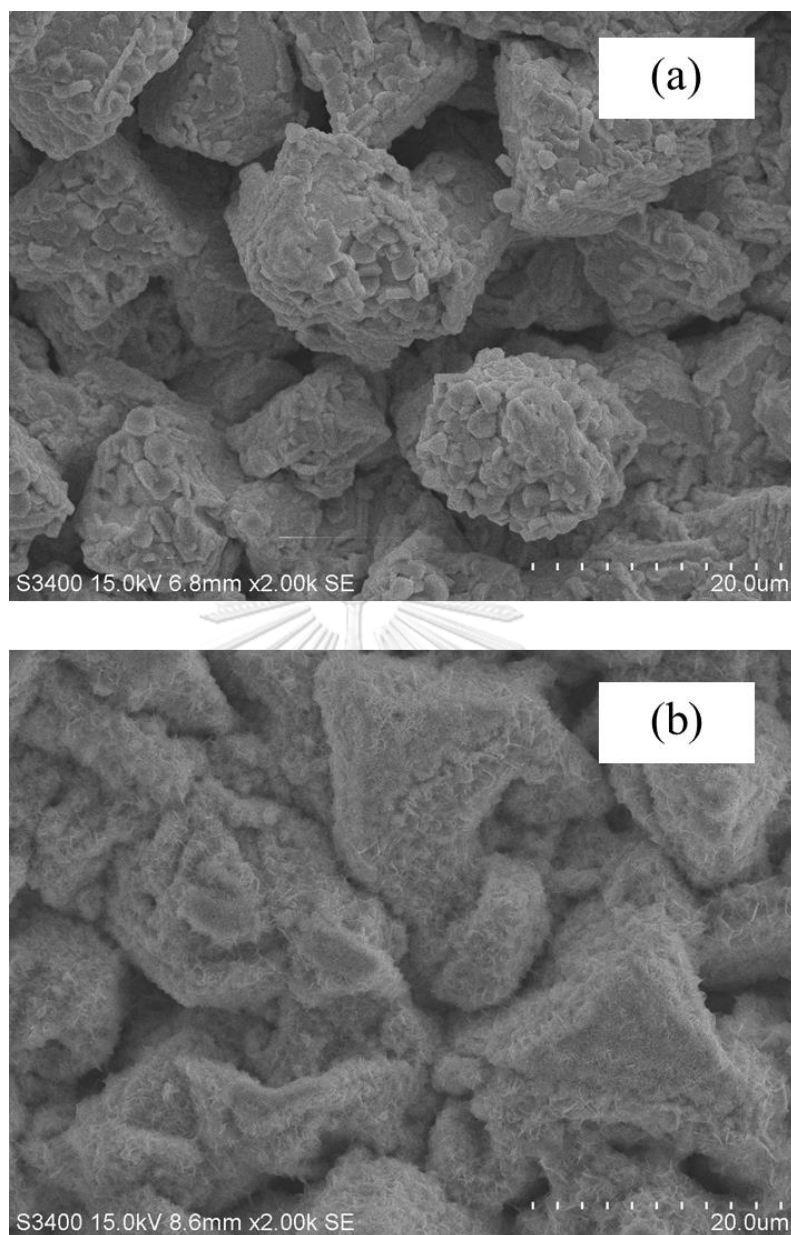


Figure 19 SEM images of Bi<sub>0.1</sub>/Cu (a) before and (b) after stability test

#### 4.3.3 X-ray diffraction (XRD) of electrocatalysts after stability test

Figure 20 shows XRD chemical compositions of  $\text{Bi}_{0.1}/\text{Cu}$  electrocatalyst before and after the stability experiment. The tetragonal  $\text{Bi}_2\text{O}_2\text{CO}_3$  diffraction peaks are found at  $23.9^\circ$ ,  $30.0^\circ$ ,  $32.7^\circ$ ,  $42.3^\circ$ , and  $56.9^\circ$ , corresponding to (011), (013), (110), (114), and (123) facets. The intensity of Bi facets after the experiments, including (012), (104), (110), (113), (202), (024), (116), and (112) planes dropped from the beginning. The results represent the formation of  $\text{Bi}_2\text{O}_2\text{CO}_3$  during the reaction tended to decline the crystallized site of Bi, causing a significant change in the morphological of the catalyst[80].

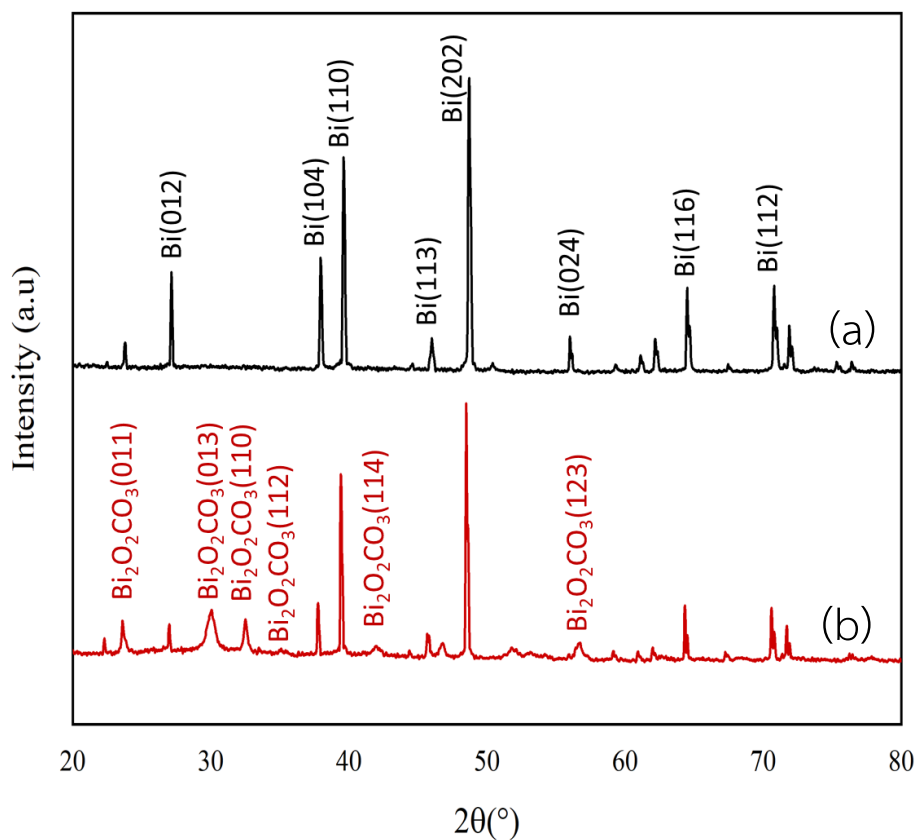


Figure 20 XRD patterns of  $\text{Bi}_{0.1}/\text{Cu}$  (a) before and (b) after stability test

## CHAPTER 5

### CONCLUSIONS

#### 5.1 Conclusions

The  $\text{Bi}_x/\text{Cu}$  and  $\text{Bi}_x\text{Sn}_y/\text{Cu}$  electrocatalysts were prepared by the electrodeposition method for electrochemical  $\text{CO}_2$  reduction reaction in an aqueous solution under ambient conditions. The morphology of deposited Bi on Cu substrate at a low and medium concentration of  $\text{Bi}^{3+}$  ion in deposition solutions (0.05 and 0.1 M) was presented as the bulky structure with different particles sizes, while the strong interaction of Bi at high concentration (0.2 M) was presented as the rough surfaces. The morphology of  $\text{Bi}_x\text{Sn}_y/\text{Cu}$  electrodes exhibited rough surface after adding Sn in the deposition solution. The effect of Bi concentration was observed to be a variation of particle sizes while the effect of adding Sn was presented in catalyst structural change leading to the reduction of the active area. In  $\text{CO}_2$ -saturated 0.1 M  $\text{KHCO}_3$ , the electrocatalysts prepared by Bi concentration of 0.1 M exhibited the maximum FE formate of about 106%. The  $\text{Bi}_{0.1}/\text{Cu}$  electrode exhibited the highest formate formation rate of  $5.41 \mu\text{mol}/\text{min}$  at  $-1.8 \text{ V}$  vs.  $\text{Ag}/\text{AgCl}$  which was 35% higher than  $\text{Bi}_{0.1}\text{Sn}_{0.025}/\text{Cu}$ , demonstrating that the Bi-bulky structure represents the outstanding performance on formate formation. Furthermore,  $\text{Bi}_{0.1}/\text{Cu}$  electrocatalyst has good stability with FE formate above 80% during 10 hours stability test. As shown by SEM images of the electrocatalysts after reaction, the morphology of the catalyst was slightly changed and Bi particle size increased. The results can be attributed to the formation of  $\text{Bi}_2\text{O}_2\text{CO}_3$  during the electrocatalytic reaction.

#### 5.2 Recommendation

1. The performance of the catalysts should be studied at other concentrations of Sn.
2. The regeneration of catalyst after electrolysis should be investigated.

## REFERENCES

1. Davis, S.J., Caldeira, K., and Matthews, H.D., Future CO<sub>2</sub> Emissions and Climate Change from Existing Energy Infrastructure. *SCIENCE*, 2010. 329: p. 1330-1333.
2. Sun, Z., et al., Fundamentals and Challenges of Electrochemical CO<sub>2</sub> Reduction Using Two-Dimensional Materials. *Chem*, 2017. 3(4): p. 560-587.
3. Qiao, J., et al., A review of catalysts for the electroreduction of carbon dioxide to produce low-carbon fuels. *Chem Soc Rev*, 2014. 43(2): p. 631-75.
4. García-Trenco, A., et al., PdIn intermetallic nanoparticles for the Hydrogenation of CO<sub>2</sub> to Methanol. *Applied Catalysis B: Environmental*, 2018. 220: p. 9-18.
5. Wu, R., et al., Hydrothermal preparation of 3D flower-like BiPO<sub>4</sub>/Bi<sub>2</sub>WO<sub>6</sub> microsphere with enhanced visible-light photocatalytic activity. *J Colloid Interface Sci*, 2018. 524: p. 350-359.
6. Shen, Q., et al., High-Yield and Selective Photoelectrocatalytic Reduction of CO<sub>2</sub> to Formate by Metallic Copper Decorated Co<sub>3</sub>O<sub>4</sub> Nanotube Arrays. *Environ Sci Technol*, 2015. 49(9): p. 5828-35.
7. Huang, X., et al., A CO<sub>2</sub> adsorption-enhanced semiconductor/metal-complex hybrid photoelectrocatalytic interface for efficient formate production. *Energy & Environmental Science*, 2016. 9(10): p. 3161-3171.
8. Kuhl, K.P., et al., New insights into the electrochemical reduction of carbon dioxide on metallic copper surfaces. *Energy & Environmental Science*, 2012. 5(5).
9. Zhang, T., et al., Bi-Modified Zn Catalyst for Efficient CO<sub>2</sub> Electrochemical Reduction to Formate. *ACS Sustainable Chemistry & Engineering*, 2019. 7(18): p. 15190-15196.
10. Zhang, Q., et al., High-selectivity electrochemical conversion of CO<sub>2</sub> to lower alcohols using a multi-active sites catalyst of transition-metal oxides. *Journal of CO<sub>2</sub> Utilization*, 2019. 34: p. 635-645.
11. Wen, G., et al., Orbital Interactions in Bi-Sn Bimetallic Electrocatalysts for Highly Selective Electrochemical CO<sub>2</sub> Reduction toward Formate Production. *Advanced Energy Materials*, 2018. 8(31).

12. Li, Q., et al., Novel Bi, BiSn, Bi<sub>2</sub>Sn, Bi<sub>3</sub>Sn, and Bi<sub>4</sub>Sn Catalysts for Efficient Electroreduction of CO<sub>2</sub> to Formic Acid. *Industrial & Engineering Chemistry Research*, 2019. 59(15): p. 6806-6814.
13. Jhong, H.-R.M., S. Ma, and P.J.A. Kenis, Electrochemical conversion of CO<sub>2</sub> to useful chemicals: current status, remaining challenges, and future opportunities. *Current Opinion in Chemical Engineering*, 2013. 2(2): p. 191-199.
14. Spinner, N.S., J.A. Vega, and W.E. Mustain, Recent progress in the electrochemical conversion and utilization of CO<sub>2</sub>. *Catal. Sci. Technol.*, 2012. 2(1): p. 19-28.
15. Zhao, M., et al., Atom vacancies induced electron-rich surface of ultrathin Bi nanosheet for efficient electrochemical CO<sub>2</sub> reduction. *Applied Catalysis B: Environmental*, 2020. 266.
16. Zhang, W., et al., Progress and Perspective of Electrocatalytic CO<sub>2</sub> Reduction for Renewable Carbonaceous Fuels and Chemicals. *Adv Sci (Weinh)*, 2018. 5(1): p. 1700275.
17. Alfath, M. and C.W. Lee, Recent Advances in the Catalyst Design and Mass Transport Control for the Electrochemical Reduction of Carbon Dioxide to Formate. *Catalysts*, 2020. 10(8).
18. Fan, M., et al., Uncovering the nature of electroactive sites in nano architected dendritic Bi for highly efficient CO<sub>2</sub> electroreduction to formate. *Applied Catalysis B: Environmental*, 2020. 274.
19. Zhong, H., et al., Bismuth nanodendrites as a high performance electrocatalyst for selective conversion of CO<sub>2</sub> to formate. *Journal of Materials Chemistry A*, 2016. 4(36): p. 13746-13753.
20. Zhang, D., et al., High efficiency and selectivity from synergy: Bi nanoparticles embedded in nitrogen doped porous carbon for electrochemical reduction of CO<sub>2</sub> to formate. *Electrochimica Acta*, 2020. 334.
21. Avila-Bolivar, B., et al., Electrochemical Reduction of CO<sub>2</sub> to Formate on Easily Prepared Carbon-Supported Bi Nanoparticles. *Molecules*, 2019. 24(11).

22. Zhang, Y., et al., Electrochemical reduction of CO<sub>2</sub> on defect-rich Bi derived from Bi<sub>2</sub>S<sub>3</sub> with enhanced formate selectivity. *Journal of Materials Chemistry A*, 2018. 6(11): p. 4714-4720.
23. An, X., et al., The in situ morphology transformation of bismuth-based catalysts for the effective electroreduction of carbon dioxide. *Sustainable Energy & Fuels*, 2020. 4(6): p. 2831-2840.
24. Lu, X., et al., Nanoporous Au-Sn with solute strain for simultaneously enhanced selectivity and durability during electrochemical CO<sub>2</sub> reduction. *Journal of Materials Science & Technology*, 2020. 43: p. 154-160.
25. Lai, Q., et al., Sn/SnO<sub>x</sub> electrode catalyst with mesoporous structure for efficient electroreduction of CO<sub>2</sub> to formate. *Applied Surface Science*, 2020. 508.
26. An, X., et al., Electrodeposition of Tin-Based Electrocatalysts with Different Surface Tin Species Distributions for Electrochemical Reduction of CO<sub>2</sub> to HCOOH. *ACS Sustainable Chemistry & Engineering*, 2019. 7(10): p. 9360-9368.
27. An, X., et al., Bi-Doped SnO Nanosheets Supported on Cu Foam for Electrochemical Reduction of CO<sub>2</sub> to HCOOH. *ACS Appl Mater Interfaces*, 2019. 11(45): p. 42114-42122.
28. Scibioh, M.A. and B. Viswanathan, Electrochemical Reduction of CO<sub>2</sub>, in *Carbon Dioxide to Chemicals and Fuels*. 2018. p. 307-371.
29. Pavesi, D., et al., CO<sub>2</sub> electroreduction on bimetallic Pd-In nanoparticles. *Catalysis Science & Technology*, 2020. 10(13): p. 4264-4270.
30. Zou, J., et al., Hierarchical architectures of mesoporous Pd on highly ordered TiO<sub>2</sub> nanotube arrays for electrochemical CO<sub>2</sub> reduction. *Journal of Materials Chemistry A*, 2020. 8(16): p. 8041-8048.
31. Gunji, T., et al., Preparation of Various Pd-Based Alloys for Electrocatalytic CO<sub>2</sub> Reduction Reaction—Selectivity Depending on Secondary Elements. *Chemistry of Materials*, 2020. 32(16): p. 6855-6863.
32. Lu, X., et al., An Integrated CO<sub>2</sub> Electrolyzer and Formate Fuel Cell Enabled by a Reversibly Restructuring Pb-Pd Bimetallic Catalyst. *Angew Chem Int Ed Engl*, 2019. 58(12): p. 4031-4035.

33. Li, J., et al., Electrohydrogenation of Carbon Dioxide using a Ternary Pd/Cu<sub>2</sub>O-Cu Catalyst. *ChemSusChem*, 2019. 12(19): p. 4471-4479.
34. Jiang, B., et al., Boosting Formate Production in Electrocatalytic CO<sub>2</sub> Reduction over Wide Potential Window on Pd Surfaces. *J Am Chem Soc*, 2018. 140(8): p. 2880-2889.
35. He, G., et al., Highly Selective and Active Pd-In/three-dimensional Graphene with Special Structure for Electroreduction CO<sub>2</sub> to Formate. *Electroanalysis*, 2018. 30(1): p. 84-93.
36. Cai, F., et al., Electrochemical promotion of catalysis over Pd nanoparticles for CO<sub>2</sub> reduction. *Chem Sci*, 2017. 8(4): p. 2569-2573.
37. Kortlever, R., et al., Electrochemical CO<sub>2</sub> Reduction to Formic Acid at Low Overpotential and with High Faradaic Efficiency on Carbon-Supported Bimetallic Pd-Pt Nanoparticles. *ACS Catalysis*, 2015. 5(7): p. 3916-3923.
38. Zhao, C., Z. Yin, and J. Wang, Efficient Electrochemical Conversion of CO<sub>2</sub> to HCOOH Using Pd-polyaniline/CNT Nanohybrids Prepared in Situ. *ChemElectroChem*, 2015. 2(12): p. 1974-1982.
39. Widiatmoko, P., et al., Electrochemical reduction of CO<sub>2</sub> to Formic Acid on Pb-Sn Alloy Cathode. *IOP Conf. Series: Materials Science and Engineering*, 2020. 823: p. 1-6.
40. Xing, Y., et al., Efficient and selective electrochemical reduction of CO<sub>2</sub> to formate on 3D porous structured multi-walled carbon nanotubes supported Pb nanoparticles. *Materials Chemistry and Physics*, 2019. 237.
41. Zhang, Z., et al., Revealing structural evolution of PbS nanocrystal catalysts in electrochemical CO<sub>2</sub> reduction using in situ synchrotron radiation X-ray diffraction. *Journal of Materials Chemistry A*, 2019. 7(41): p. 23775-23780.
42. Wu, H., et al., Design of naturally derived lead phytate as an electrocatalyst for highly efficient CO<sub>2</sub> reduction to formic acid. *Green Chemistry*, 2018. 20(20): p. 4602-4606.



43. Wu, H., et al., Highly efficient electrochemical reduction of CO<sub>2</sub> into formic acid over lead dioxide in an ionic liquid–catholyte mixture. *Green Chemistry*, 2018. 20(8): p. 1765-1769.
44. Chen, L., et al., Electrochemical Reduction of CO<sub>2</sub> with an Oxide-Derived Lead Nano-Coralline Electrode in Dimcarb. *ChemElectroChem*, 2017. 4(6): p. 1402-1410.
45. Yadav, V.S.K. and M.K. Purkait, Synthesis of Pb<sub>2</sub>O electrocatalyst and its application in the electrochemical reduction of CO<sub>2</sub> to HCOOH in various electrolytes. *RSC Advances*, 2015. 5(50): p. 40414-40421.
46. He, Z., et al., Electrochemically created roughened lead plate for electrochemical reduction of aqueous CO<sub>2</sub>. *Catalysis Communications*, 2015. 72: p. 38-42.
47. KOLELI, F., et al., Electrochemical reduction of CO<sub>2</sub> at Pb- and Sn-electrodes in a fixed-bed reactor in aqueous K<sub>2</sub>CO<sub>3</sub> and KHCO<sub>3</sub> media. *Applied Electrochemistry*, 2003. 33: p. 447–450.
48. Yuan, X., et al., Decoration of In nanoparticles on In<sub>2</sub>S<sub>3</sub> nanosheets enables efficient electrochemical reduction of CO<sub>2</sub>. *Chem Commun (Camb)*, 2020. 56(30): p. 4212-4215.
49. Zha, B., C. Li, and J. Li, Efficient electrochemical reduction of CO<sub>2</sub> into formate and acetate in polyoxometalate catholyte with indium catalyst. *Journal of Catalysis*, 2020. 382: p. 69-76.
50. Bohlen, B., et al., Electrochemical CO<sub>2</sub> reduction to formate on indium catalysts prepared by electrodeposition in deep eutectic solvents. *Electrochemistry Communications*, 2020. 110.
51. Zhu, M., et al., Structure-Tunable Copper-Indium Catalysts for Highly Selective CO<sub>2</sub> Electroreduction to CO or HCOOH. *ChemSusChem*, 2019. 12(17): p. 3955-3959.
52. Hegner, R., L.F.M. Rosa, and F. Harnisch, Electrochemical CO<sub>2</sub> reduction to formate at indium electrodes with high efficiency and selectivity in pH neutral electrolytes. *Applied Catalysis B: Environmental*, 2018. 238: p. 546-556.

53. Birdja, Y.Y., et al., Effects of Substrate and Polymer Encapsulation on CO<sub>2</sub> Electroreduction by Immobilized Indium(III) Protoporphyrin. *ACS Catal*, 2018. 8(5): p. 4420-4428.
54. Sun, X., et al., MoP Nanoparticles Supported on Indium-Doped Porous Carbon: Outstanding Catalysts for Highly Efficient CO<sub>2</sub> Electroreduction. *Angew Chem Int Ed Engl*, 2018. 57(9): p. 2427-2431.
55. Rabiee, A. and D. Nematollahi, Electrochemical reduction of CO<sub>2</sub> to formate ion using nanocubic mesoporous In(OH)<sub>3</sub>/carbon black system. *Materials Chemistry and Physics*, 2017. 193: p. 109-116.
56. Bitar, Z., et al., Electrocatalytic reduction of carbon dioxide on indium coated gas diffusion electrodes—Comparison with indium foil. *Applied Catalysis B: Environmental*, 2016. 189: p. 172-180.
57. Larrazábal, G.O., et al., Synergistic effects in silver–indium electrocatalysts for carbon dioxide reduction. *Journal of Catalysis*, 2016. 343: p. 266-277.
58. Huang, J., et al., A renewable, flexible and robust single layer nitrogen-doped graphene coating Sn foil for boosting formate production from electrocatalytic CO<sub>2</sub> reduction. *Journal of CO<sub>2</sub> Utilization*, 2019. 33: p. 166-170.
59. Lim, J., et al., Electrochemically deposited Sn catalysts with dense tips on a gas diffusion electrode for electrochemical CO<sub>2</sub> reduction. *Journal of Materials Chemistry A*, 2020. 8(18): p. 9032-9038.
60. Jiang, X., et al., A highly selective tin-copper bimetallic electrocatalyst for the electrochemical reduction of aqueous CO<sub>2</sub> to formate. *Applied Catalysis B: Environmental*, 2019. 259.
61. Kim, Y.E., et al., Leaching-resistant SnO<sub>2</sub>/γ-Al<sub>2</sub>O<sub>3</sub> nanocatalyst for stable electrochemical CO<sub>2</sub> reduction into formate. *Journal of Industrial and Engineering Chemistry*, 2019. 78: p. 73-78.
62. Rasul, S., et al., Low cost and efficient alloy electrocatalysts for CO<sub>2</sub> reduction to formate. *Journal of CO<sub>2</sub> Utilization*, 2019. 32: p. 1-10.

63. Wang, X., et al., Nanoporous Ag-Sn derived from codeposited AgCl-SnO<sub>2</sub> for the electrocatalytic reduction of CO<sub>2</sub> with high formate selectivity. *Electrochemistry Communications*, 2019. 102: p. 52-56.
64. Liu, S., et al., Stable nanoporous Sn/SnO<sub>2</sub> composites for efficient electroreduction of CO<sub>2</sub> to formate over wide potential range. *Applied Materials Today*, 2018. 13: p. 135-143.
65. Yadav, V.S.K., et al., Synthesis of Sn catalysts by solar electro-deposition method for electrochemical CO<sub>2</sub> reduction reaction to HCOOH. *Catalysis Today*, 2018. 303: p. 276-281.
66. Li, F., et al., Towards a better Sn: Efficient electrocatalytic reduction of CO<sub>2</sub> to formate by Sn/SnS<sub>2</sub> derived from SnS<sub>2</sub> nanosheets. *Nano Energy*, 2017. 31: p. 270-277.
67. Wang, Y., et al., Electrochemical reduction of CO<sub>2</sub> to formate catalyzed by electroplated tin coating on copper foam. *Applied Surface Science*, 2016. 362: p. 394-398.
68. Zhao, C. and J. Wang, Electrochemical reduction of CO<sub>2</sub> to formate in aqueous solution using electro-deposited Sn catalysts. *Chemical Engineering Journal*, 2016. 293: p. 161-170.
69. Fu, Y., et al., Electrochemical CO<sub>2</sub> reduction to formic acid on crystalline SnO<sub>2</sub> nanosphere catalyst with high selectivity and stability. *Chinese Journal of Catalysis*, 2016. 37(7): p. 1081-1088.
70. Zhang, R., et al., Electrochemical reduction of CO<sub>2</sub> on SnO<sub>2</sub>/nitrogen-doped multiwalled carbon nanotubes composites in KHCO<sub>3</sub> aqueous solution. *Materials Letters*, 2015. 141: p. 63-66.
71. Del Castillo, A., et al., Electrocatalytic reduction of CO<sub>2</sub> to formate using particulate Sn electrodes: Effect of metal loading and particle size. *Applied Energy*, 2015. 157: p. 165-173.
72. Zhang, R., W. Lv, and L. Lei, Role of the oxide layer on Sn electrode in electrochemical reduction of CO<sub>2</sub> to formate. *Applied Surface Science*, 2015. 356: p. 24-29.

73. Jiang, H., et al., High-selectivity electrochemical CO<sub>2</sub> reduction to formate at low overpotential over Bi catalyst with hexagonal sheet structure. *Applied Surface Science*, 2021. 541.
74. Wu, D., et al., Boosting formate production at high current density from CO<sub>2</sub> electroreduction on defect-rich hierarchical mesoporous Bi/Bi<sub>2</sub>O<sub>3</sub> junction nanosheets. *Applied Catalysis B: Environmental*, 2020. 271.
75. Subramanian, S., et al., Bismuth Oxychloride Dispersed on Nitrogen-Doped Carbon as Catalyst for the Electrochemical Reduction of CO<sub>2</sub> to Formate. *ChemElectroChem*, 2020. 7(10): p. 2265-2273.
76. Yang, Q., et al., Novel Bi-Doped Amorphous SnO<sub>x</sub> Nanoshells for Efficient Electrochemical CO<sub>2</sub> Reduction into Formate at Low Overpotentials. *Adv Mater*, 2020. 32(36): p. e2002822.
77. Zhou, J.H., et al., Boosting Electrochemical Reduction of CO<sub>2</sub> at a Low Overpotential by Amorphous Ag-Bi-S-O Decorated Bi(0) Nanocrystals. *Angew Chem Int Ed Engl*, 2019. 58(40): p. 14197-14201.
78. Díaz-Sainz, G., et al., CO<sub>2</sub> electroreduction to formate: Continuous single-pass operation in a filter-press reactor at high current densities using Bi gas diffusion electrodes. *Journal of CO<sub>2</sub> Utilization*, 2019. 34: p. 12-19.
79. Su, P., et al., Ultrathin Bismuth Nanosheets as a Highly Efficient CO<sub>2</sub> Reduction Electrocatalyst. *ChemSusChem*, 2018. 11(5): p. 848-853.
80. Zhang, X., et al., Polyethylene glycol induced reconstructing Bi nanoparticle size for stabilized CO<sub>2</sub> electroreduction to formate. *Journal of Catalysis*, 2018. 365: p. 63-70.
81. Bertin, E., et al., Selective electroreduction of CO<sub>2</sub> to formate on Bi and oxide-derived Bi films. *Journal of CO<sub>2</sub> Utilization*, 2017. 19: p. 276-283.
82. Zhang, X., et al., Enhancing CO<sub>2</sub> electrolysis to formate on facilely synthesized Bi catalysts at low overpotential. *Applied Catalysis B: Environmental*, 2017. 218: p. 46-50.

83. Gamburg, Y.D. and G. Zangari, Introduction to Electrodeposition: Basic Terms and Fundamental Concepts. Theory and Practice of Metal Electrodeposition, 2011: p. 1-25.
84. Saji, V.S. and R. Cook, Electrodeposition: the versatile technique for nanomaterials. Corrosion protection and control using nanomaterials, 2012: p. 86-125.
85. Tsai, Y.-D., C.-C. Hu, and C.-C. Lin, Electrodeposition of Sn–Bi lead-free solders: Effects of complex agents on the composition, adhesion, and dendrite formation. *Electrochimica Acta*, 2007. 53(4): p. 2040-2047.
86. Sandnes, E., et al., Electrodeposition of bismuth from nitric acid electrolyte. *Electrochimica Acta*, 2007. 52(21): p. 6221-6228.
87. Özdemir, R. and İ.H. Karahan, Effect of solution Zn concentration on electrodeposition of  $Cu_xZn_{1-x}$  alloys: materials and resistivity characterisation. *Transactions of the IMF*, 2019. 97(2): p. 95-99.
88. Halpern, J. Sizes of Atoms and Ions. 2021; Available from: <https://chem.libretexts.org/@go/page/21739>.
89. Peng, Y. and K. Deng, Fabrication of reduced graphene oxide nanosheets reinforced Sn–Bi nanocomposites by electro-chemical deposition. *Composites Part A: Applied Science and Manufacturing*, 2015. 73: p. 55-62.
90. Chiew Ying Heong, H., Goh Yingxin, Lee Seen Fang, Effects of Sn Concentration and Current Density on Sn-Bi Electrodeposition in Additive Free Plating Bath. 4th Asia Symposium on Quality Electronic Design, 2012: p. 286-290.
91. Lee, Y.-G., et al., Electrodeposition of the Sn-58 wt.%Bi layer for low-temperature soldering. *Metals and Materials International*, 2011. 17(1): p. 117-121.
92. Determination of EMF of a Cell. 2013; Available from: [amrita.olabs.edu.in/?sub=73&brch=8&sim=153&cnt=1](http://amrita.olabs.edu.in/?sub=73&brch=8&sim=153&cnt=1)
93. Derma, F. Cell EMF Calculator. 2020; Available from: <https://www.omnicalculator.com/chemistry/electromotive-force>.

94. Li, X., et al., Activation of amorphous bismuth oxide via plasmonic Bi metal for efficient visible-light photocatalysis. *Journal of Catalysis*, 2017. 352: p. 102-112.
95. Yoo, J.S., et al., Theoretical Insight into the Trends that Guide the Electrochemical Reduction of Carbon Dioxide to Formic Acid. *ChemSusChem*, 2016. 9(4): p. 358-63.
96. Hatsukade, T., et al., Insights into the electrocatalytic reduction of CO(2) on metallic silver surfaces. *Phys Chem Chem Phys*, 2014. 16(27): p. 13814-9.
97. Kendra P. Kuhl, E.R.C., David N. Abram, Thomas F. Jaramillo, Supporting Information for: New insights into the electrochemical reduction of carbon dioxide on metallic copper surfaces. *Electronic Supplementary Material (ESI) for Energy & Environmental Science* This journal is © The Royal Society of Chemistry 2012: p. s1-s11.



## APPENDIX

### A. The calibration curve of gas product

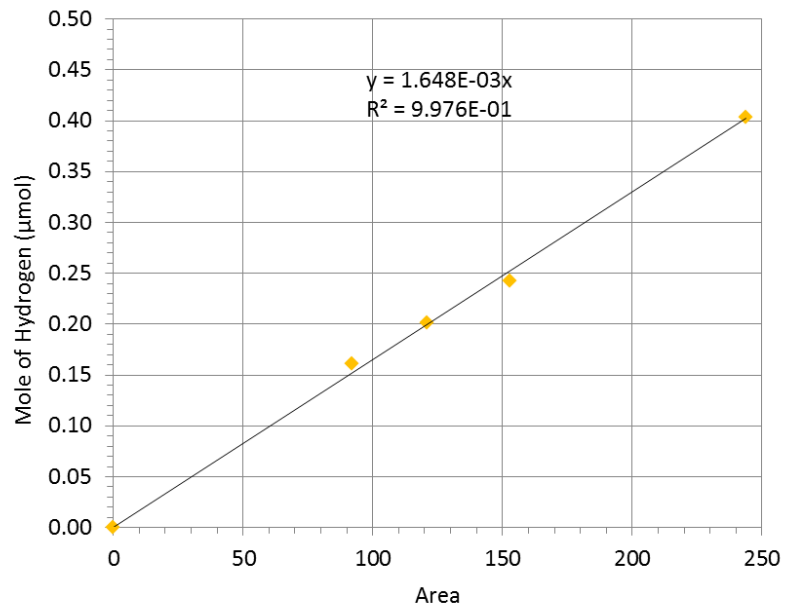


Figure A1 The calibration curve of H<sub>2</sub>

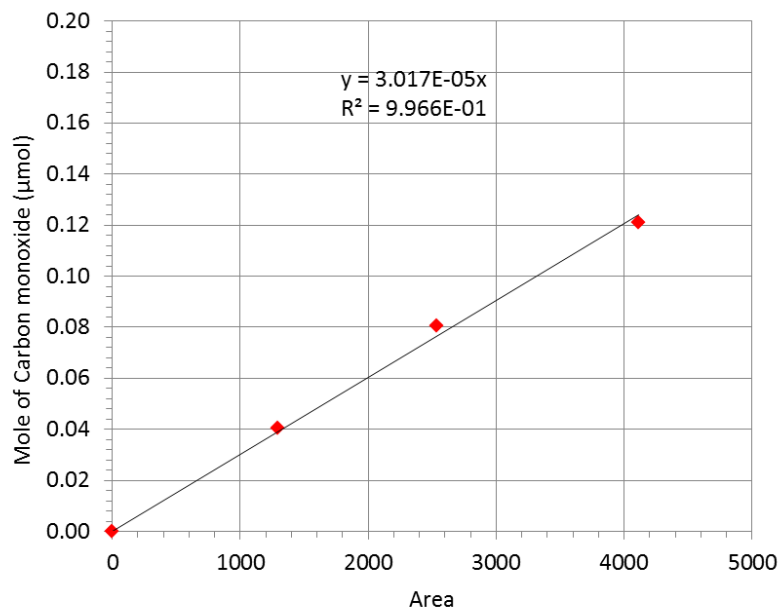


Figure A2 The calibration curve of CO

## B. The liquid product identification for NMR analysis

Table B The liquid product identification for NMR analysis. [97]

Product name	<sup>1</sup> H splitting	Chemical Shift
Formate	s	8.33
DMSO (Internal Standard)	s	2.6

## C. The Faraday Efficiency (FE)

The performance of the process is evaluated by the FE.

$$FE(\%) = \frac{z \cdot n \cdot F}{q} \times 100$$

Where,

z : electrons exchanged to form the product

n : moles product

F : Faraday constant = 96,485 C/mol

q : the total charge or power applied in process.



## VITA

**NAME** Jutamas Wasombut

**DATE OF BIRTH** 22 September 1996

**PLACE OF BIRTH** Chiang rai, Thailand

**INSTITUTIONS ATTENDED** B.Sc. Chemical Technology, Faculty of Science,  
Chulalongkorn University

**HOME ADDRESS** 11 Police Residence, Muangmai-Maptaphut 7 Rd, T.  
Hauypong, A. Muang, Rayong 21150.



จุฬาลงกรณ์มหาวิทยาลัย  
**CHULALONGKORN UNIVERSITY**